



UNIVERSIDADE ESTADUAL DE CAMPINAS  
SISTEMA DE BIBLIOTECAS DA UNICAMP  
REPOSITÓRIO DA PRODUÇÃO CIENTÍFICA E INTELLECTUAL DA UNICAMP

**Versão do arquivo anexado / Version of attached file:**

Versão do Editor / Published Version

**Mais informações no site da editora / Further information on publisher's website:**

<https://iopscience.iop.org/article/10.3847/1538-4365/ab13a8/meta>

**DOI: 10.3847/1538-4365/ab13a8**

**Direitos autorais / Publisher's copyright statement:**

©2019 by Institute of Physics Publishing. All rights reserved.

DIRETORIA DE TRATAMENTO DA INFORMAÇÃO

Cidade Universitária Zeferino Vaz Barão Geraldo


CEP 13083-970 – Campinas SP

Fone: (19) 3521-6493

<http://www.repositorio.unicamp.br>



# Spectral Analysis and New Visible and Ultraviolet Lines of Ar V

C. J. B. Pagan<sup>1</sup> , M. Raineri<sup>2</sup>, M. Gallardo<sup>2</sup>, and J. Reyna Almandos<sup>2</sup>

<sup>1</sup> School of Electrical and Computer Engineering, University of Campinas (UNICAMP), 13083-970, Campinas, SP, Brazil; [cesarpagan@fee.unicamp.br](mailto:cesarpagan@fee.unicamp.br)

<sup>2</sup> Centro de Investigaciones Ópticas (CIOp), CC 3, 1897, Gonnet, La Plata, Argentina

Received 2018 December 17; revised 2019 March 15; accepted 2019 March 25; published 2019 June 12

## Abstract

A capillary discharge tube was used to record the Ar spectrum in the region of 330–4400 Å. We analyzed a set of 109 lines of Ar V, with 10 of them being classified for the first time. Part of these newly identified lines (six in total) corresponds to electric dipole transitions in the visible and ultraviolet regions of the spectrum. We calculated weighted transition rates ( $gA$ ) for all experimentally observed lines and the corresponding lifetimes using a relativistic Hartree–Fock method with configuration interaction. The equations were modified to consider core polarization (CP) effects. A study on the Si isoelectronic sequence found that considering CP effects is essential for the correct description of the Ar V structure.

*Key words:* atomic data – line: identification – ultraviolet: general

## 1. Introduction

Wright (1920) was the first to observe a line of four times ionized argon (Ar V) as a very faint line from the planetary nebula (PN) NGC 7027. Later, Stoy (1934) and Bowen (1935) identified this line as belonging to a set of forbidden transitions between levels of ground configuration with wavelengths in the visible region of the spectrum. Other observations for this set came from astrophysical sources (Bowen 1960; Penston et al. 1983; McKenna et al. 1997), including ultraviolet and visible lines. The fine structure mid-infrared lines for  $^3P_1-^3P_2$  and  $^3P_0-^3P_1$  transitions were determined also from observations of the PN NGC 7027 (Kelly & Lacy 1995; Feuchtgruber et al. 1997).

Ar V was observed for the first time in a laboratory by Boyce (1935) using an electrodeless discharge and later by Phillips & Parker (1941) using a spark gap as a light source in the vacuum ultraviolet region. All subsequent experimental contributions were made exclusively in the region of the spectrum below 1500 Å using theta-pinch (Fawcett et al. 1978), capillary discharge (Jiang et al. 1984; Lévêque et al. 1984; Cavalcanti et al. 1995, 1996), and a high-voltage open spark (Raassen et al. 1992) as spectroscopic light sources. Livingston et al. (1981) compiled the experimental data available for lifetimes of Ar V levels, all of them for transitions with ground configuration levels.

Kohstall et al. (1998) calculated lifetimes for Si-like ions using a multiconfigurational Dirac–Fock approach. Froese Fischer et al. (2006) made an extensive calculation for lifetimes and transition probabilities from Be-like to Ne-like sequences up to  $Z = 26$ , using the multiconfigurational Hartree–Fock method (MCHF) to determine radial functions, with relativistic effects through the Breit–Pauli Hamiltonian. We compare our results for lifetimes with those of Froese Fischer et al. (2006). More recently, Tayal et al. (2009) calculated lifetimes for Ar V levels using configuration–interaction wavefunctions obtained from the code of Hibbert (1975).

In our study, we report the experimental analysis of six new Ar V lines that are the first classification of electric dipole transitions in the ultraviolet and visible region for this spectrum. To date, astronomical observations of Ar V from the surface of the earth were only possible through forbidden

transitions, whose values of weighted transition rates ( $gA$ ) are typically weaker than those of allowed transitions. Another four lines classified for the first time are in the vacuum ultraviolet region.

The Ar<sup>4+</sup> occurrence in nebulae requires a high-temperature central star to provide photons with enough energy to produce the ionization required. This is the case of nebulae with intermediary mass stars as a progenitor. In those cases, argon is considered a good tracer for the abundance of alpha species in PNs, since it remains unchanged during the nucleosynthesis processes occurring along AGB stellar evolution (Werner et al. 2007), with the advantage that it is not depleted into dust because of its chemical properties. Nevertheless, ionization coefficient factors (ICFs) for argon, used for abundance calculations, provide extremely uncertainty in cases of ionized nebulae, as found in recent investigations by Delgado-Inglada et al. (2014). New data on this element may remove this objection.

We found that the inclusion of core polarization (CP) made the “obs.–calc.” curves for the isoelectronic sequence much smoother, so we could accept new experimental achievements. This inclusion was crucial for a correct spectroscopic analysis, at least in this case. Section 2 shows the Hartree–Fock equations, modified to include CP.

We used a capillary discharge tube built at CIOp for our experimental observations. Our early study (Borges et al. 2005) describes the experimental setup, the materials, and the methods used to classify lines and determine energy levels.

In this study, lines in the vacuum region are below 2100 Å and have an uncertainty estimated at  $\pm 0.02$  Å. Above this value, air wavelengths are estimated to be correct at  $\pm 0.01$  Å.

## 2. Theory

The method used here is different from our previous works (Raineri et al. 2012; Gallardo et al. 2015; Raineri et al. 2017) since we have changed the equations used for solve the Hartree–Fock + Core Polarization calculations. In this study, we modified the Cowan’s atomic calculation package, described in described in Cowan (1981)’s book “The Theory of Atomic Structure and Spectra,” from this point on referred to as TASS, for the inclusion of the polarization potentials.

### 2.1. Modification of the Hartree–Fock Equations for the Inclusion of CP Effects

CP effects (see, for example, Curtis 2003) considers the deformation of the atomic core by the electric field of the outermost electrons.

Using the electric field as in Baylis (1977) and Migdalek & Baylis (1978),

$$\mathbf{E}(\mathbf{r}) = \frac{\mathbf{r}}{(r^2 + r_c^2)^{3/2}}, \quad (1)$$

CP effects are appropriately included into the atomic Hamiltonian by the addition of the one-particle

$$V_{P1} = -\alpha_d \sum_{i=1}^N \frac{r_i^2}{(r_i^2 + r_c^2)^3} \quad (2)$$

and the two-particle

$$V_{P2} = -\alpha_d \sum_{i>j}^N \frac{\mathbf{r}_i \cdot \mathbf{r}_j}{(r_i^2 + r_c^2)^{3/2} (r_j^2 + r_c^2)^{3/2}} \quad (3)$$

operators, where  $\alpha_d$  is the dipole polarizability of the core, the sum is over all  $N$  electrons of the atom,  $r_k$  ( $k = i, j$ ) is the radial coordinate of electron  $k$ , and  $r_c$  is the cut-off radius that is barely the core radius. The inclusion of those operators in the Hamiltonian leads us to the modified form of Hartree–Fock equations:

$$\begin{aligned} & \left[ -\frac{d^2}{dr^2} + \frac{l_i(l_i + 1)}{r^2} - \frac{2Z}{r} - \frac{\alpha_d r^2}{(r^2 + r_c^2)^3} + \sum_{j=1}^q (w_j - \delta_{ij}) \right. \\ & \times \int_0^\infty \frac{2}{r} P_{n_j l_j}^2(r_2) dr_2 - (w_i - 1) A_i(r) \left. \right] P_{n_i l_i}(r) \\ & = \epsilon_i P_{n_i l_i}(r) + \sum_{j \neq i}^q w_j [\delta_{l_i l_j} \epsilon_{ij} + C_{ij, \alpha_d}(r)] P_{n_j l_j}(r) \\ A_i(r) & = \frac{2l_i + 1}{4l_i + 1} \sum_{k>0} \begin{pmatrix} l_i & k & l_i \\ 0 & 0 & 0 \end{pmatrix}^2 \\ & \times \int_0^\infty 2 \begin{bmatrix} r < \\ r > \end{bmatrix} P_{n_i l_i}(r') P_{n_i l_i}(r') dr' \\ C_{ij, \alpha_d}(r) & = \frac{1}{2} \sum_k \begin{pmatrix} l_i & k & l_j \\ 0 & 0 & 0 \end{pmatrix}^2 \\ & \times \int_0^\infty 2 \begin{bmatrix} r < \\ r > \end{bmatrix} + \delta_{k,1} \frac{\alpha_d r r'}{(r^2 + r_c^2)^{3/2} (r'^2 + r_c^2)^{3/2}} \left. \right] \\ & \times P_{n_j l_j}(r') P_{n_i l_i}(r') dr' \end{aligned} \quad (4)$$

which guided us in the adaptation of the program RCN (TASS, pp. 456–461), version Mod 36, and calculated the radial wavefunctions. Here, we have  $q$ -occupied orbitals,  $P_{nl}$  are the radial functions for  $nl$  orbitals, and the coefficients  $3j$  are as defined in TASS. In this study, Equation (4) replaces Equations (7.11)–(7.14) of TASS in the calculations with the inclusion of CP effects.

The reduced matrix element was replaced by

$$\begin{aligned} \int_0^\infty P_{nl}(r) r P_{n'l'}(r) dr & \rightarrow \int_0^\infty P_{nl}(r) r \cdot \left[ 1 - \frac{\alpha_d}{(r^2 + r_c^2)^{3/2}} \right] \\ & \times P_{n'l'}(r) dr - \frac{\alpha_d}{r_c^3} \int_0^{r_c} P_{nl}(r) r P_{n'l'}(r) dr, \end{aligned} \quad (5)$$

which is the same modification used by Quinet et al. (1999, 2002) and Biémont et al. (2000a, 2000b) to correct transition matrix elements when including CP and core penetration effects.

### 3. Atomic Structure and Transition Rates

We performed relativistic Hartree–Fock (HFR) and HFR including core polarization ( $V_{P1}$  and  $V_{P2}$ ) potentials (HFR+CP) calculations using the Cowan’s Atomic Package modified as described above. As our base for eigenvectors, we select the configurations with single–double (SD; see Froese Fischer et al. 1997) substitutions for (even)  $3s^2 3p^2$  and (odd parity)  $3s 3p^3$  belonging to the  $\{3\}^4$  and  $\{3\}^3 \{4\}^1$  complexes (configurations with a neon core plus four  $n = 3$  orbitals or three  $n = 3$  and one  $n = 4$  orbitals), following the discussion of Froese Fischer et al. (2006) for the Si-like sequence. Moreover, we added configurations with  $n = 5$  orbitals due to the value of their energy levels, their mix with the configurations under study, and the information available from the transitions involving these levels. The set as a whole has 22 even ( $3s^2 3p^2$ ,  $3s 3p^2 3d$ ,  $3p^4$ ,  $3s^2 3p 4p$ ,  $3s 3p^2 4s$ ,  $3s^2 3p 4f$ ,  $3s^2 3d^2$ ,  $3s^2 3p 5p$ ,  $3s^2 3p 5f$ ,  $3s 3p^2 4d$ ,  $3s^2 3d 4s$ ,  $3s 3p^2 5s$ ,  $3p^3 4p$ ,  $3s^2 3d 4d$ ,  $3s 3p 3d 4p$ ,  $3p^2 3d^2$ ,  $3p^3 4f$ ,  $3s 3d^3$ ,  $3s 3p 3d 4f$ ,  $3p^2 3d 4s$ ,  $3s 3d^2 4s$ , and  $3s 3d^2 4d$ ) and 25 odd ( $3s 3p^3$ ,  $3s^2 3p 3d$ ,  $3s^2 3p 4s$ ,  $3s^2 3p 4d$ ,  $3p^3 3d$ ,  $3s^2 3p 5s$ ,  $3s 3p 3d^2$ ,  $3p^3 4s$ ,  $3p^3 4d$ ,  $3p^3 5s$ ,  $3p 3d^3$ ,  $3s 3p 3d 4s$ ,  $3s 3p 3d 4d$ ,  $3s 3p 3d 5s$ ,  $3p 3d^2 4s$ ,  $3p 3d^2 4d$ ,  $3s^2 3d 4p$ ,  $3s 3d^2 4p$ ,  $3d^3 4p$ ,  $3s 3p^2 4p$ ,  $3p^2 3d 4p$ ,  $3s 3p^2 4f$ ,  $3s 3d^2 4f$ ,  $3s^2 3d 4f$ , and  $3p^2 3d 4f$ ) configurations.

Using this same basis of configurations, we made calculations replacing HF energy parameters—that is, energy average, electrostatic integrals, and spin–orbit energy parameters—by those adjusted to fit the experimental energy values using the procedure described in TASS pp. 468–476. We made these calculations with and without CP effects. It is noteworthy that only parameters belonging to configurations with known experimental levels can be adjusted; the remaining parameters were left to 100% of their HFR or HFR+CP values. With the adjusted values we calculated the energy; lifetime and composition of the levels; as well as the weighted transition probability rate,  $gA$ ; and weighted oscillator strengths,  $gf$ , as defined in Equations (14.33), (14.38), and (14.42) of TASS.

The value of the weighted transition probability rate  $gA_{\gamma J, \gamma' J'}$  for a transition from an upper level  $\gamma J$  (quantum numbers  $\gamma$  and total angular momentum  $J$ ) to a lower level  $\gamma' J'$ , obtained from Equations (14.33) and (14.42) of TASS, in units of  $s^{-1}$ , is given by

$$\begin{aligned} gA_{\gamma J, \gamma' J'} & = (2J + 1) A_{\gamma J, \gamma' J'} \\ & = \frac{64\pi^4 e^2 a_0^2 \sigma^3}{3h} \left| \sum_{\beta} \sum_{\beta'} y_{\beta J}^{\gamma} y_{\beta' J'}^{\gamma'} \langle \beta J || \mathbf{P}^{(1)} || \beta' J' \rangle \right|^2. \end{aligned} \quad (6)$$

Here, the eigenvector components are given by their respective expansion coefficients,  $y_{\beta J}^{\gamma}$  and  $y_{\beta' J'}^{\gamma'}$ , for basis components,  $\beta$  and  $\beta'$ , of a single configuration basis, where  $\sigma = (E_{\gamma J} - E_{\gamma' J'})/hc$  is the wavenumber,  $E_{\gamma J}$  is the eigenvalue for the upper energy level, and  $E_{\gamma' J'}$  is for the lower energy level,  $h$  is the Planck's constant,  $e$  is the elementary charge of the electron,  $a_0$  is the Bohr radius, and  $\langle \beta J || \mathbf{P}^{(1)} || \beta' J' \rangle$  is the electric dipole reduced matrix element for the transition  $\beta J - \beta' J'$ .

An equation relates the weighted emission transition probability rates,  $gA$ , to the weighted absorption oscillator strengths,  $gf$  (TASS, Equation (14.38)):

$$gA = (2J + 1)A_{\gamma J, \gamma' J'} = \frac{8\pi^2 e^2}{mc} \sigma^2 gf$$

$$= 0.66702 \sigma^2 (2J' + 1) f_{\gamma' J', \gamma J}, \quad (7)$$

which we write here for convenience. Here,  $\sigma$  is the wavenumber in  $\text{cm}^{-1}$ . As usual in spectroscopic jargon, “ $g$ ” has different meanings for  $gA$  and  $gf$ : in the former,  $g = (2J + 1)$  is the degeneracy of the upper energy state, while in the latter,  $g = (2J' + 1)$  is the corresponding degeneracy for the lower energy state.

### 3.1. Polarizability $\alpha_d$ and Cut-off Radius $r_c$ for Ar V

We considered the core-valence correlation using a CP potential model as described above, which is a method that demands knowledge about the polarizability and the cut-off radius of the core. The value of  $\alpha_d$  for Ar V core—that is, for  $\text{Ar}^{8+}$ —is not available in Fraga & Muszyńska (1981)’s table, but a numerical extrapolation of the isoelectronic sequence contained there gives us a value near  $0.037 a_0^3$ . This finding agrees with the one calculated by Johnson et al. (1983) as  $0.0371 a_0^3$  and later by Koch & Andrae (2011), who found  $\alpha_d = 0.0373 a_0^3$ .

We also calculated our own value for the polarization constant in order to improve our understanding of core-valence correlation effects from the formula

$$\alpha_d = 4\text{Ry}^2 \sum_{\gamma J}^M f_{\gamma' J', \gamma J} \lambda_{\gamma' J', \gamma J}^2, \quad (8)$$

where  $f_{\gamma' J', \gamma J}$  is the (absorption) oscillator strength for the transition  $\gamma' J' \rightarrow \gamma J$ ,  $\lambda_{\gamma' J', \gamma J}$  is its corresponding wavelength, and  $\text{Ry} = 109,737.316 \text{ cm}^{-1}$  is the Rydberg constant. We followed the method described in our previous study (Raineri et al. 2012) and found the limit curve defined by Equation (3) contained therein, resulting in  $\alpha_d = 0.036 a_0^3$ . Transition oscillator strengths to the ground state  $1s^2 2s^2 2p^6 \ ^1S_0$  are calculated from a set of all configurations that corresponds to all SD substitutions from ground state to odd configurations of the  $2p^5 \{3, 4\}^1$  and  $2p^4 \{3, 4\}^2$  complexes, excluding the  $4f$  orbital, plus the Rydberg series  $2p^5 ns$  and  $2p^5 nd$ , with  $n = 5$  to  $M$  ( $M = 10$  for  $s$  series and  $28$  for  $d$  series). Ground was described by the addition of single excitation states,  $2s^2 2p^5 np$  ( $n = 3-9$ ) and  $2s 2p^6 ms$  ( $m = 3-5$ ).

The potential model requires a cut-off parameter that distinguishes between core and valence regions. Usually, we consider the mean radius of the outermost core orbital, but by analyzing the shape of the wavefunctions, we see a region

where both core amplitudes decrease and valence amplitudes increase around  $r_c = 0.5 a_0$  (Figure 1).

### 3.2. Isoelectronic Calculations

Ar V belongs to the silicon isoelectronic sequence. In our study, we considered the 12 first ions of this sequence (from Si I to Mn XII) and used a set with 24 even configurations ( $3s^2 3p^2$ ,  $3s 3p^2 3d$ ,  $3p^4$ ,  $3s^2 3p 4p$ ,  $3s 3p^2 4s$ ,  $3s^2 3p 4f$ ,  $3s^2 3d^2$ ,  $3s^2 3p 5p$ ,  $3s^2 3p 5f$ ,  $3s 3p^2 4d$ ,  $3s^2 3d 4s$ ,  $3s 3p^2 5s$ ,  $3p^3 4p$ ,  $3s^2 3d 4d$ ,  $3s 3p 3d 4p$ ,  $3p^2 3d^2$ ,  $3p^3 4f$ ,  $3s 3d^3$ ,  $3s 3p 3d 4f$ ,  $3p^2 3d 4s$ ,  $3s 3d^2 4s$ ,  $3s 3d^2 4d$ ,  $3s^2 3p 6p$ , and  $3s^2 3p 6f$ ) and 25 odd configurations ( $3s 3p^3$ ,  $3s^2 3p 3d$ ,  $3s^2 3p 4s$ ,  $3s^2 3p 4d$ ,  $3p^3 3d$ ,  $3s^2 3p 5s$ ,  $3s 3p 3d^2$ ,  $3p^3 4s$ ,  $3p^3 4d$ ,  $3p^3 5s$ ,  $3p 3d^3$ ,  $3s 3p 3d 4s$ ,  $3s 3p 3d 4d$ ,  $3s 3p 3d 5s$ ,  $3p 3d^2 4s$ ,  $3p 3d^2 4d$ ,  $3s^2 3d 4p$ ,  $3s 3d^2 4p$ ,  $3d^3 4p$ ,  $3s 3p^2 4p$ ,  $3p^2 3d 4p$ ,  $3s 3p^2 4f$ ,  $3s^2 3p 5d$ ,  $3s^2 3p 6s$ , and  $3s^2 3p 6d$ ). This set is somewhat different from the set described in the Section 3 for Ar V in order to study the levels that are important for other elements of the Si I sequence.

We made HFR and HFR+CP calculations to compare their results. HFR+CP calculations used values for  $\alpha_d$  based on polynomial interpolation of the values by Koch & Andrae (2011). Values for  $r_c$  are obtained with the same criteria as described in Section 3.1, also by polynomial interpolation. See Table 1 for the values used.

## 4. Analysis

Our analysis consider the experimental observation of first and second order lines and their intensity as a function of discharge characteristics (energy and pressure), as well as Ritz combinations of energy levels and line intensity comparisons with their respective theoretical transition rates. Computational techniques supported our analysis through least-squares adjustment, as described in TASS, and through isoelectronic trends to study the difference between the observed and calculated (“obs.–calc.”) values of energy levels and wavelengths for the Si-like sequence.

Table 2 shows the experimental wavelengths and weighted transition probabilities ( $gA$ ) for all known Ar V electric dipole (E1) transitions. The  $gA$  values in this table are from HFR and HFR+CP calculations, made with and without energy parameters adjusted by least-squares fitting. Table 3 presents experimental energy levels, their composition, and lifetimes obtained from the same calculations. We can also see in Table 3 that the values for lifetimes of this study are, in general, greater than those found by Froese Fischer et al. (2006).

### 4.1. Least-squares Fitting

In this study, we use both an HFR+CP calculation and a usual HFR as a starting point to compare the two methods. Only the parameters directly related to the configurations that are dominant in the experimental levels description were adjusted; the rest of them remained fixed. Tables 4 and 5 show the result of these adjustments.

In the single configuration model—which corresponds to the HF equations that Cowan’s package solves—the contribution of  $V_{p2}$  has the same symmetry that is produced by the  $G^1$  integrals for the Hamiltonian. This contribution does not change the value of the  $G^1$  integrals directly but causes a modification in the fields that are absorbed by all parameters, including the  $G^1$  integral itself. Note that the adjusted values for  $F^k$  and  $G^k$  are, in general, closer to their theoretical values for

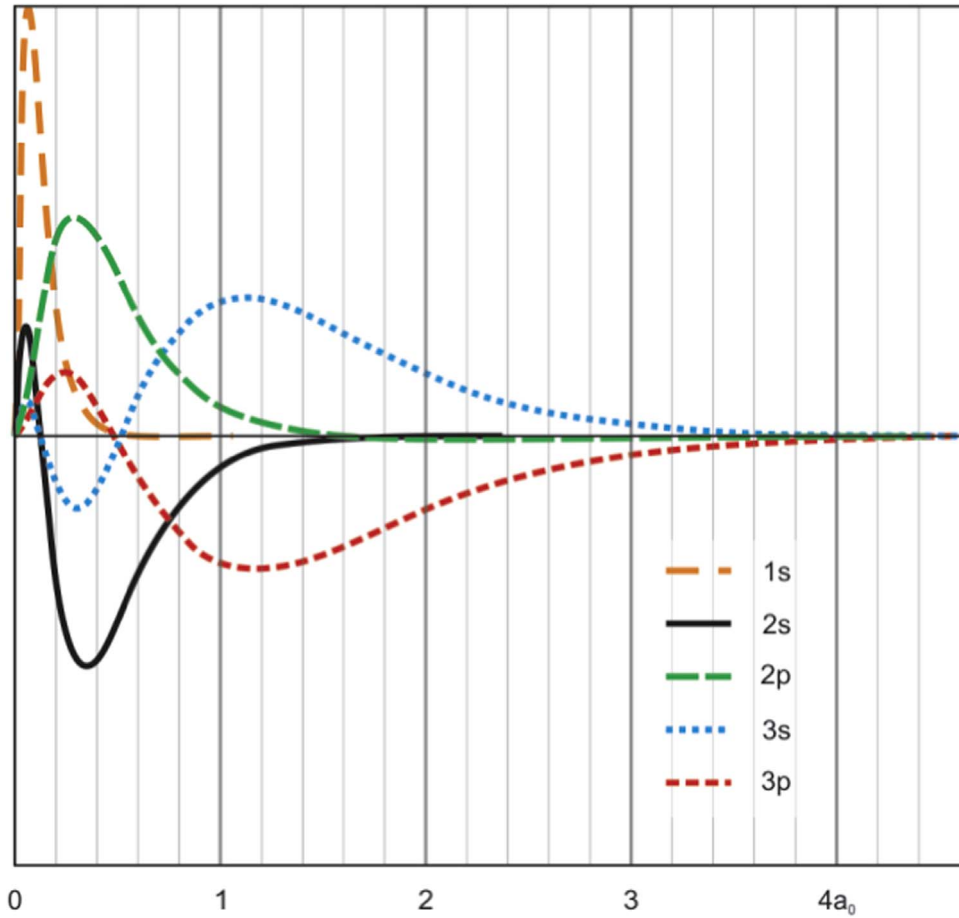


Figure 1. Radial wavefunctions of Ar V. The radial component for the 3s and 3p orbitals crosses the  $r$ -axis approximately in  $r = 0.5a_0$ .

Table 1

Values for Polarizability  $\alpha_d$  and Cut-off Radius  $r_c$  for Silicon Isoelectronic Calculation from Si I to Mn XII

Ion	$\alpha_d (a_0^3)$	$r_c (a_0)$
Si I	0.16273	0.70002
P II	0.10607	0.62962
S III	0.07238	0.57615
Cl IV	0.05121	0.53415
Ar V	0.03733	0.49948
K VI	0.02789	0.46918
Ca VII	0.02127	0.44128
Sc VIII	0.01652	0.41466
Ti IX	0.01304	0.38890
V X	0.01043	0.36404
Cr XI	0.00845	0.34052
Mn XII	0.00691	0.31893

HFR+CP than those for HFR (the contrary is valid for only 4 in 25 integrals). We can interpret this finding if we consider that the scaling factor for electrostatic integrals comes from unconsidered correlation effects that are partially supplied by the inclusion of CP in the Hamiltonian. The adjustments produced similar values for the final standard deviation.

We excluded the level  $3p5s:1P_1$  from least-squares calculations since it did not produce reasonable parameters from its fitting. Fawcett et al. (1978) classified this level at  $432,378 \text{ cm}^{-1}$  as an attempt from only one line. When excluding this level from the fitting, the least-squares calculation predicts a value around

$1300 \text{ cm}^{-1}$  greater for  $1P_1$  level. Figure 2 shows a plot of the difference between values observed and calculated of the intervals  $3P_1 - 1P_1$  and  $3P_2 - 1P_1$  for the isoelectronic sequence of Si I. All elements with experimental data available are shown. If we had used the value predicted by the software, the points corresponding to Ar V would appear near the horizontal axis. In this case, a line near  $282 \text{ \AA}$  will represent the transition of  $3p^2:1D_2 - 3p5s:1P_1$  and the line at  $240.339 \text{ \AA}$  should be considered misclassified. However, this wavelength is out of the range of our spectrographs, and we could not verify this possibility. We conclude that this classification is a still open question.

#### 4.2. Lifetimes

Table 3 shows the lifetimes of known levels. The values are for the four calculations presented in this study, i.e., HFR and HFR + CP, with and without adjustment of the energy parameters for the experimental levels and the published lifetimes by Froese Fischer et al. (2006), which are generally close and somewhat lower than our findings. This last comment is also valid for a comparison of our results with those obtained by Kohstall et al. (1998).

Table 6 shows the experimental lifetimes obtained by Livingston et al. (1981) for some terms of the  $3s3p^3$  and  $3p3d$  configurations, as well as the values calculated by us using HFR + CP and HFR + CP (adjusted) and those published by Froese Fischer et al. (2006). Calculated values are weight-averaged from the levels to obtain the corresponding term lifetime using

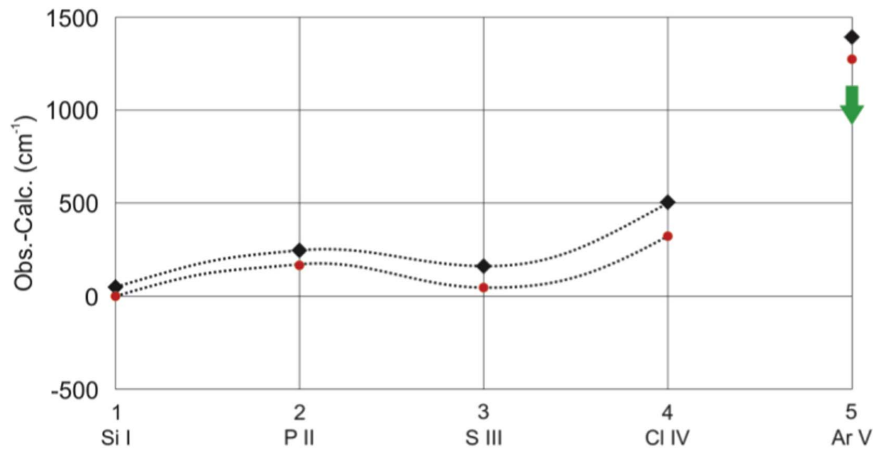


**Figure 2.** Configuration  $3p5s$ . Isoelectronic trend of observed–calculated values for the intervals  ${}^3P_1-{}^1P_1$  (circles) and  ${}^3P_2-{}^1P_1$  (diamonds). When we replace the experimental value from Fawcett et al. (1978) by the value predicted by the software, the points for Ar V tend to decrease by around  $1300\text{ cm}^{-1}$ .

the formula  $\tau \approx (\sum_J(2J+1))/\sum_J((2J+1)/\tau_J)$  (provided that the values of  $\tau_J$  are close to each other) in order to compare the experimental and calculated values. Here,  $J$  is the total angular momentum of the level,  $\tau_J$  is its corresponding lifetime,  $\tau$  is the term lifetime, and the sums are over all possible values of  $J$  of the term.

#### 4.3. New Lines in the Visible and Ultraviolet Region

We classified a set of six E1 lines between 2432.99 and 4391.16 Å for the first time. The  $3p^4$  configuration (here identified as  $3s3p^23d$ , see Section 4.6) participates in all transitions; the odd parity configurations involved are  $3p3d$  and  $3p4s$ . For these lines, excluding the line 2432.99 Å, the statistical correlation (Pagan et al. 2011) between the observed intensity and  $gA$  values is 0.94, which reinforces our identifications. Since these transitions are not known for other ions, we did not study the isoelectronic trend of these lines along the sequence.

The values of  $gA$  for these lines are all around  $10^5\text{ s}^{-1}$ , which is much stronger than the visible and ultraviolet lines classified before the present work, whose transitions had values of  $gA$  no higher than  $2\text{ s}^{-1}$  (see Froese Fischer et al. 2006). The reason for such difference is that the five lines in the visible–ultraviolet known prior to this study (Bowen 1960; Penston et al. 1983; McKenna et al. 1997) are dipole magnetic or quadrupole electric transitions, which are typically much weaker than the electric dipole transitions reported here. However, the reader should consider that the intensity of a spontaneous emission line depends not only on the value of  $gA$  but also on the population of the upper state, which is a characteristic of the plasma.

#### 4.4. New Lines in the Vacuum Ultraviolet

Another four lines were classified for the first time. Two lines are with ground configuration levels—that is, 479.83 Å  $3p^2: {}^3P_2-3p3d\ {}^3D_3$  and 796.99 Å  $3p^2: {}^1D_2-3s3p^3\ {}^3P_1$ . We observed a good agreement with the isoelectronic trend for these lines, as we can see in Figures 3 and 4 for the curve representing the wavenumber divided by the number of the spectrum ( $\zeta$ , the Roman numeral in front of the symbol of the element). Others are with  $3s3p^23d$  excited configuration—that is, 607.01 Å  $3s3p^2({}^3P)3d: {}^3P_1-3p5s\ {}^3P_1$  and 1423.91 Å

$3s3p^3: {}^1P_1-3s3p^2({}^3P)3d\ {}^3P_1$ —for which there is no experimental data to allow an isoelectronic trend analysis.

#### 4.5. The Importance of CP in the Isoelectronic Trend of Silicon

We analyzed the isoelectronic trend of the difference between observed (experimental) values and calculated ab-initio values of the energy levels—that is, “obs.–calc.”—for the first 12 elements of the silicon sequence.

A comparison between isoelectronic analysis with and without CP effects included in the Hamiltonian showed significant differences for most levels studied. For the  $3p3p^3$  configuration, the “obs.–calc.” values of  ${}^3P_{0,1,2}$ ,  ${}^3D_{1,2,3}$ , and  ${}^1D_2$  levels of Ar V appear displaced from the soft curves that describe the sequences when using HFR theoretical values, while it fits perfectly if we use HFR+CP instead. The only exception is for  ${}^3P_0$  for a small displacement. The same happens for  ${}^3D_{1,2,3}$  and  ${}^1F_3$  levels of the configuration  $3p3d$ . As we can see in Figures 5 and 6, the inclusion of CP effects may change our judgment about what is a good classification.

Strong configuration interactions are present in the composition of the  $3p3d: {}^3P_{0,1,2}$  levels of P II and S III, producing a discontinuous curve for these ions. Notwithstanding, the conclusion is similar to the other levels mentioned above. We also analyzed the  $3p3d: {}^1P_1$  level, but in this case, the result was only a reduction in the deviation.

The isoelectronic study for  $3p3d$  configuration, Figure 6, also helped us predict the energy levels of three times ionized chlorine (Cl IV),  ${}^1F_3$  ( $203,040 \pm 300\text{ cm}^{-1}$ ) and  ${}^1P_1$  ( $209,000 \pm 1100\text{ cm}^{-1}$ ) that are still unclassified.

#### 4.6. The $3p^4-3s3p^23d$ Interaction

Except for Ar V and Ca VII (Levashov & Struk 1996), experimental classification of levels of the  $3p^4$  configuration are absent of all ions of the Si-like sequence, which prevents the analysis of the isoelectronic trend of its values. This configuration was first classified for Ar V by Cavalcanti et al. (1996) and is present in the homologous Kr V spectrum as  $4p^4$  (Rezende et al. 2010), where it interacts strongly with the  $4s4p^24d$  levels (Raineri et al. 2012).

Such as the Kr V spectrum, the interaction  $3p^4-3s3p^23d$  for Ar V is significant. Before least-square adjustment calculations, greatest components have contributions close to 50%; after adjustment,  $3p^4$  levels appear to belong to the  $3s3p^23d$

**Table 2**  
Transition Rates for Ar V

Int <sup>b</sup>	Experiment				Designation			HFR+CP $gA_{ji}$ <sup>a</sup>		HFR $gA_{ji}$ <sup>a</sup>		References	
	$\lambda$ (Å)	unc. (Å)	$E_i$ ( $10^3 \text{ cm}^{-1}$ )	$E_j$ ( $10^3 \text{ cm}^{-1}$ )			Adjusted ( $\text{s}^{-1}$ )	( $\text{s}^{-1}$ )	Adjusted ( $\text{s}^{-1}$ )	( $\text{s}^{-1}$ )			
[ ]	231.868	0.006	0.763	–	432.044	$3p^2 \ ^3P_1$	–	$3p5s \ ^3P_2$	4.284E+09	3.695E+09	4.143E+09	3.624E+09	F1978
[1]	232.379	0.006	0.000	–	430.331	$3p^2 \ ^3P_0$	–	$3p5s \ ^3P_1$	3.100E+09	3.079E+09	2.764E+09	2.997E+09	F1978
[4]	232.549	0.006	2.029	–	432.044	$3p^2 \ ^3P_2$	–	$3p5s \ ^3P_2$	1.281E+10	1.181E+10	1.240E+10	1.148E+10	F1978
[1t]	240.339	0.006	16.299	–	432.378	$3p^2 \ ^1D_2$	–	$3p5s \ ^1P_1$	1.740E+10	1.862E+10	1.916E+08	1.797E+10	F1978
[bl]	248.489	0.006	0.763	–	403.185	$3p^2 \ ^3P_1$	–	$3p4d \ ^3P_1$	4.620E+08	4.562E+08	3.752E+08	3.669E+08	F1978
[4]	249.611	0.006	2.029	–	402.652	$3p^2 \ ^3P_2$	–	$3p4d \ ^3P_2$	1.827E+09	1.872E+09	1.484E+09	1.503E+09	F1978
[3]	251.115	0.006	0.763	–	398.987	$3p^2 \ ^3P_1$	–	$3p4d \ ^3F_2$	9.438E+08	1.421E+09	7.316E+08	1.210E+09	F1978
[5t]	251.544	0.006	0.000	–	397.545	$3p^2 \ ^3P_0$	–	$3p4d \ ^3D_1$	1.526E+09	1.523E+09	1.243E+09	1.226E+09	F1978
[5]	251.599	0.006	2.029	–	399.487	$3p^2 \ ^3P_2$	–	$3p4d \ ^3F_3$	1.867E+09	2.536E+09	1.452E+09	2.146E+09	F1978
[6 <sup>+</sup> ]	252.072	0.006	0.763	–	397.545	$3p^2 \ ^3P_1$	–	$3p4d \ ^3D_1$	8.621E+08	8.811E+08	7.051E+08	7.088E+08	F1978
[6 <sup>+</sup> ]	252.072	0.006	0.763	–	397.476	$3p^2 \ ^3P_1$	–	$3p4d \ ^3D_2$	2.383E+09	1.940E+09	1.977E+09	1.498E+09	F1978
[6]	252.671	0.006	2.029	–	397.800	$3p^2 \ ^3P_2$	–	$3p4d \ ^3D_3$	3.813E+09	3.176E+09	3.182E+09	2.453E+09	F1978
[7]	257.495	0.006	16.299	–	404.656	$3p^2 \ ^1D_2$	–	$3p4d \ ^1F_3$	4.692E+09	4.409E+09	3.658E+09	3.265E+09	F1978
[8 <sup>+</sup> ]	262.2	0.1	16.299	–	397.800	$3p^2 \ ^1D_2$	–	$3p4d \ ^3D_3$	2.346E+07	1.601E+07	1.583E+07	1.070E+07	L1984
[8 <sup>+</sup> ]	262.2	0.1	16.299	–	397.545	$3p^2 \ ^1D_2$	–	$3p4d \ ^3D_1$	2.764E+05	2.048E+04	2.874E+05	6.372E+04	L1984
[8 <sup>+</sup> ]	262.2	0.1	16.299	–	397.476	$3p^2 \ ^1D_2$	–	$3p4d \ ^3D_2$	1.524E+07	4.426E+07	9.586E+06	4.333E+07	L1984
[7]	322.019	0.006	85.851	–	396.391	$3s3p^3 \ ^5S_2$	–	$3p^2 4s \ ^5P_3$	4.253E+10	4.286E+10	4.286E+10	4.150E+10	F1978
[6]	323.152	0.006	85.851	–	395.303	$3s3p^3 \ ^5S_2$	–	$3p^2 4s \ ^5P_2$	3.003E+10	3.025E+10	3.025E+10	2.929E+10	F1978
[5]	323.939	0.006	85.851	–	394.551	$3s3p^3 \ ^5S_2$	–	$3p^2 4s \ ^5P_1$	1.787E+10	1.800E+10	1.800E+10	1.743E+10	F1978
1	336.57	0.01	0.763	–	297.878	$3p^2 \ ^3P_1$	–	$3p4s \ ^3P_2$	1.330E+10	1.362E+10	1.318E+10	1.332E+10	C1995
1	337.58	0.01	0.000	–	296.231	$3p^2 \ ^3P_0$	–	$3p4s \ ^3P_1$	1.024E+10	1.062E+10	1.012E+10	1.038E+10	C1995
1	338.01	0.01	2.029	–	297.878	$3p^2 \ ^3P_2$	–	$3p4s \ ^3P_2$	3.908E+10	4.014E+10	3.870E+10	3.923E+10	C1995
1	338.45	0.01	0.763	–	296.231	$3p^2 \ ^3P_1$	–	$3p4s \ ^3P_1$	7.441E+09	7.779E+09	7.336E+09	7.604E+09	C1995
1	339.02	0.01	0.763	–	295.731	$3p^2 \ ^3P_1$	–	$3p4s \ ^3P_0$	1.033E+10	1.061E+10	1.023E+10	1.037E+10	C1995
1	339.89	0.01	2.029	–	296.231	$3p^2 \ ^3P_2$	–	$3p4s \ ^3P_1$	1.293E+10	1.325E+10	1.280E+10	1.295E+10	C1995
2	350.88	0.01	16.299	–	301.290	$3p^2 \ ^1D_2$	–	$3p4s \ ^1P_1$	4.853E+10	4.981E+10	4.778E+10	4.884E+10	C1995
1	357.23	0.01	16.299	–	296.231	$3p^2 \ ^1D_2$	–	$3p4s \ ^3P_1$	1.533E+09	9.543E+08	1.689E+09	9.239E+08	C1995
3	379.69	0.01	37.912	–	301.290	$3p^2 \ ^1S_0$	–	$3p4s \ ^1P_1$	8.741E+09	8.728E+09	8.817E+09	8.730E+09	C1995
[2]	389.163	0.006	154.211	–	411.173	$3p3d \ ^1D_2$	–	$3s3p^2 \ (^3P)3d \ ^1F_3$	1.600E+11	1.738E+11	1.585E+11	1.760E+11	F1978
[7]	400.0	0.1	2.029	–	252.141	$3p^2 \ ^3P_2$	–	$3p3d \ ^1P_1$	8.950E+05	4.244E+05	8.398E+05	4.293E+05	L1984
1	411.01	0.01	2.029	–	245.328	$3p^2 \ ^3P_2$	–	$3p3d \ ^1F_3$	4.730E+08	2.664E+08	4.943E+08	2.757E+08	C1995
3	436.63	0.01	16.299	–	245.328	$3p^2 \ ^1D_2$	–	$3p3d \ ^1F_3$	1.933E+11	2.208E+11	1.990E+11	2.287E+11	C1995
3	445.97	0.01	0.000	–	224.219	$3p^2 \ ^3P_0$	–	$3p3d \ ^3D_1$	3.834E+10	4.458E+10	3.932E+10	4.624E+10	C1995
2	446.96	0.01	0.763	–	224.498	$3p^2 \ ^3P_1$	–	$3p3d \ ^3D_2$	8.674E+10	1.007E+11	8.909E+10	1.044E+11	C1995
3	447.53	0.01	0.763	–	224.219	$3p^2 \ ^3P_1$	–	$3p3d \ ^3D_1$	3.569E+10	4.027E+10	3.703E+10	4.174E+10	C1995
2	449.08	0.01	2.029	–	224.706	$3p^2 \ ^3P_2$	–	$3p3d \ ^3D_3$	1.778E+11	2.039E+11	1.836E+11	2.115E+11	C1995
3	449.50	0.01	2.029	–	224.498	$3p^2 \ ^3P_2$	–	$3p3d \ ^3D_2$	4.140E+10	4.600E+10	4.320E+10	4.769E+10	C1995
2	450.079	0.020	2.029	–	224.219	$3p^2 \ ^3P_2$	–	$3p3d \ ^3D_1$	3.451E+09	3.728E+09	3.642E+09	3.859E+09	P1941
3	452.39	0.01	0.763	–	221.815	$3p^2 \ ^3P_1$	–	$3p3d \ ^1D_2$	3.920E+08	1.556E+07	3.634E+08	5.758E+07	C1995
2	454.99	0.01	2.029	–	221.815	$3p^2 \ ^3P_2$	–	$3p3d \ ^1D_2$	3.099E+08	2.496E+08	2.922E+08	2.583E+08	C1995
3	458.09	0.01	0.000	–	218.287	$3p^2 \ ^3P_0$	–	$3p3d \ ^3P_1$	2.109E+10	2.310E+10	2.203E+10	2.395E+10	C1995
3	458.96	0.01	0.763	–	218.647	$3p^2 \ ^3P_1$	–	$3p3d \ ^3P_0$	1.654E+10	1.880E+10	1.709E+10	1.949E+10	C1995

**Table 2**  
(Continued)

Int <sup>b</sup>	Experiment				Designation			HFR+CP $gA_{ji}$ <sup>a</sup>		HFR $gA_{ji}$ <sup>a</sup>		References	
	$\lambda$ (Å)	unc. (Å)	$E_i$ ( $10^3 \text{ cm}^{-1}$ )	$E_j$ ( $10^3 \text{ cm}^{-1}$ )				Adjusted ( $\text{s}^{-1}$ )	( $\text{s}^{-1}$ )	Adjusted ( $\text{s}^{-1}$ )	( $\text{s}^{-1}$ )		
3	459.73	0.01	0.763	–	218.287	$3p^2 \ ^3P_1$	–	$3p3d \ ^3P_1$	8.889E+09	1.058E+10	9.010E+09	1.099E+10	C1995
2	461.24	0.01	0.763	–	217.572	$3p^2 \ ^3P_1$	–	$3p3d \ ^3P_2$	2.931E+10	3.226E+10	3.075E+10	3.338E+10	C1995
2	462.41	0.01	2.029	–	218.287	$3p^2 \ ^3P_2$	–	$3p3d \ ^3P_1$	1.939E+10	2.245E+10	1.998E+10	2.326E+10	C1995
3	463.94	0.01	2.029	–	217.572	$3p^2 \ ^3P_2$	–	$3p3d \ ^3P_2$	5.145E+10	6.007E+10	5.276E+10	6.229E+10	C1995
1	466.79	0.01	37.912	–	252.141	$3p^2 \ ^1S_0$	–	$3p3d \ ^1P_1$	6.604E+10	7.249E+10	6.832E+10	7.492E+10	C1995
3	486.57	0.01	16.299	–	221.815	$3p^2 \ ^1D_2$	–	$3p3d \ ^1D_2$	1.062E+11	1.210E+11	1.112E+11	1.252E+11	C1995
1	495.09	0.01	16.299	–	218.287	$3p^2 \ ^1D_2$	–	$3p3d \ ^3P_1$	9.726E+07	7.406E+07	1.047E+08	7.489E+07	C1995
2[37]	496.84	0.02	16.299	–	217.572	$3p^2 \ ^1D_2$	–	$3p3d \ ^3P_2$	1.288E+09	4.886E+08	1.262E+09	6.120E+08	J1984
2	511.89	0.01	0.000	–	195.356	$3p^2 \ ^3P_0$	–	$3s3p^3 \ ^1P_1$	2.849E+08	1.908E+08	2.960E+08	1.821E+08	C1995
3[50]	513.889	0.002	0.763	–	195.356	$3p^2 \ ^3P_1$	–	$3s3p^3 \ ^1P_1$	1.121E+09	7.773E+08	1.167E+09	7.594E+08	R1992
3[25]	517.254	0.002	2.029	–	195.356	$3p^2 \ ^3P_2$	–	$3s3p^3 \ ^1P_1$	8.134E+08	5.211E+08	8.295E+08	5.006E+08	R1992
3[150]	522.0940	0.002	0.000	–	191.537	$3p^2 \ ^3P_0$	–	$3s3p^3 \ ^3S_1$	6.817E+09	7.794E+09	7.097E+09	8.087E+09	R1992
3[250]	524.1817	0.002	0.763	–	191.537	$3p^2 \ ^3P_1$	–	$3s3p^3 \ ^3S_1$	1.983E+10	2.277E+10	2.063E+10	2.365E+10	R1992
3[300]	527.685	0.002	2.029	–	191.537	$3p^2 \ ^3P_2$	–	$3s3p^3 \ ^3S_1$	3.305E+10	3.749E+10	3.438E+10	3.896E+10	R1992
2	536.75	0.01	37.912	–	224.219	$3p^2 \ ^1S_0$	–	$3p3d \ ^3D_1$	4.073E+06	1.993E+06	3.885E+06	2.113E+06	C1995
1bl	546.18	0.02	141.771	–	324.862	$3s3p^3 \ ^3P_1$	–	$3s3p^2 \ (^1D)3d \ ^1S_0$	1.084E+07	1.301E+07	1.065E+07	1.299E+07	C1996
3[250]	558.477	0.002	16.299	–	195.356	$3p^2 \ ^1D_2$	–	$3s3p^3 \ ^1P_1$	2.749E+10	3.143E+10	2.864E+10	3.273E+10	R1992
2[80]	570.656	0.002	16.299	–	191.537	$3p^2 \ ^1D_2$	–	$3s3p^3 \ ^3S_1$	6.307E+08	4.129E+08	6.417E+08	3.941E+08	R1992
[13]	602.97	0.02	245.328	–	411.173	$3p3d \ ^1F_3$	–	$3s3p^2 \ (^3P)3d \ ^1F_3$	2.256E+10	9.572E+09	3.101E+10	9.237E+09	J1984
4[150]	635.152	0.002	37.912	–	195.356	$3p^2 \ ^1S_0$	–	$3s3p^3 \ ^1P_1$	2.183E+09	2.398E+09	2.247E+09	2.634E+09	R1992
2	650.95	0.01	37.912	–	191.537	$3p^2 \ ^1S_0$	–	$3s3p^3 \ ^3S_1$	6.417E+07	3.928E+07	6.508E+07	4.007E+07	C1995
3	651.68	0.01	0.763	–	154.211	$3p^2 \ ^3P_1$	–	$3p3d \ ^1D_2$	5.707E+06	6.344E+06	6.452E+06	6.435E+06	C1995
4	692.29	0.02	121.629	–	266.075	$3s3p^3 \ ^3D_1$	–	$3s3p^2 \ (^3P)3d \ ^3P_0$	2.616E+08	1.321E+09	2.956E+08	1.393E+09	C1996
3	694.65	0.02	121.629	–	265.588	$3s3p^3 \ ^3D_1$	–	$3s3p^2 \ (^3P)3d \ ^3P_1$	1.755E+08	1.012E+09	1.980E+08	1.069E+09	C1996
4q	694.85	0.02	121.675	–	265.588	$3s3p^3 \ ^3D_2$	–	$3s3p^2 \ (^3P)3d \ ^3P_1$	6.059E+08	2.969E+09	6.857E+08	3.131E+09	C1996
3	700.51	0.02	121.675	–	264.430	$3s3p^3 \ ^3D_2$	–	$3s3p^2 \ (^3P)3d \ ^3P_2$	1.636E+08	1.037E+09	1.843E+08	1.095E+09	C1996
3q	701.12	0.02	121.803	–	264.430	$3s3p^3 \ ^3D_3$	–	$3s3p^2 \ (^3P)3d \ ^3P_2$	1.125E+09	5.595E+09	1.273E+09	5.900E+09	C1996
4[150]	705.364	0.002	0.000	–	141.771	$3p^2 \ ^3P_0$	–	$3s3p^3 \ ^3P_1$	7.117E+08	7.403E+08	7.433E+08	7.962E+08	R1992
2	708.57	0.01	0.763	–	141.893	$3p^2 \ ^3P_1$	–	$3s3p^3 \ ^3P_0$	7.123E+08	7.410E+08	7.444E+08	7.978E+08	C1995
4qw[250]	709.190	0.002	0.763	–	141.771	$3p^2 \ ^3P_1$	–	$3s3p^3 \ ^3P_1$	6.167E+08	6.366E+08	6.485E+08	6.852E+08	R1992
5[250]	709.230	0.002	0.763	–	141.763	$3p^2 \ ^3P_1$	–	$3s3p^3 \ ^3P_2$	7.806E+08	8.163E+08	8.103E+08	8.790E+08	R1992
4qw[200]	715.600	0.002	2.029	–	141.771	$3p^2 \ ^3P_2$	–	$3s3p^3 \ ^3P_1$	7.829E+08	8.210E+08	8.141E+08	8.857E+08	R1992
5[150]	715.640	0.002	2.029	–	141.763	$3p^2 \ ^3P_2$	–	$3s3p^3 \ ^3P_2$	2.647E+09	2.749E+09	2.767E+09	2.964E+09	R1992
4q[3]	720.9	0.1	264.430	–	403.185	$3s3p^2 \ (^3P)3d \ ^3P_2$	–	$3p4d \ ^3P_1$	1.673E+07	1.407E+07	1.761E+07	1.419E+07	L1984
4[100]	725.097	0.002	16.299	–	154.211	$3p^2 \ ^1D_2$	–	$3p3d \ ^1D_2$	4.130E+09	3.658E+09	4.170E+09	4.068E+09	R1992
3	772.16	0.02	195.356	–	324.862	$3s3p^3 \ ^1P_1$	–	$3s3p^2 \ (^1D)3d \ ^1S_0$	3.138E+08	1.209E+09	3.899E+08	1.287E+09	C1996
4	804.46	0.02	154.211	–	278.523	$3p3d \ ^1D_2$	–	$3s3p^2 \ (^1D)3d \ ^1D_2$	2.593E+09	4.439E+09	2.902E+09	4.654E+09	C1996
4	815.23	0.02	141.763	–	264.430	$3s3p^3 \ ^3P_2$	–	$3s3p^2 \ (^3P)3d \ ^3P_2$	4.146E+06	4.058E+08	5.354E+06	4.359E+08	C1996
4*	815.23	0.02	141.771	–	264.430	$3s3p^3 \ ^3P_1$	–	$3s3p^2 \ (^3P)3d \ ^3P_2$	1.087E+06	1.477E+08	1.336E+06	1.588E+08	C1996
4[200]	822.160	0.002	0.000	–	121.629	$3p^2 \ ^3P_0$	–	$3s3p^3 \ ^3D_1$	4.141E+08	3.820E+08	4.317E+08	4.165E+08	R1992
4[250]	827.048	0.002	0.763	–	121.675	$3p^2 \ ^3P_1$	–	$3s3p^3 \ ^3D_2$	9.156E+08	8.470E+08	9.538E+08	9.235E+08	R1992
4qw[150]	827.353	0.002	0.763	–	121.629	$3p^2 \ ^3P_1$	–	$3s3p^3 \ ^3D_1$	2.565E+08	2.357E+08	2.645E+08	2.575E+08	R1992



**Table 2**  
(Continued)

Int <sup>b</sup>	Experiment			Designation				HFR+CP $gA_{ji}$ <sup>a</sup>		HFR $gA_{ji}$ <sup>a</sup>		References	
	$\lambda$ (Å)	unc. (Å)	$E_i$ ( $10^3$ cm <sup>-1</sup> )	$E_j$ ( $10^3$ cm <sup>-1</sup> )				Adjusted (s <sup>-1</sup> )	(s <sup>-1</sup> )	Adjusted (s <sup>-1</sup> )	(s <sup>-1</sup> )		
4qw[200]	834.903	0.002	2.029	–	121.803	$3p^2 \ ^3P_2$	–	$3s3p^3 \ ^3D_3$	1.535E+09	1.425E+09	1.592E+09	1.554E+09	R1992
4d[50]	835.799	0.002	2.029	–	121.675	$3p^2 \ ^3P_2$	–	$3s3p^3 \ ^3D_2$	2.084E+08	1.912E+08	2.124E+08	2.092E+08	R1992
4[100]	836.112	0.002	2.029	–	121.629	$3p^2 \ ^3P_2$	–	$3s3p^3 \ ^3D_1$	1.223E+07	1.099E+07	1.237E+07	1.205E+07	R1992
3	897.85	0.02	154.211	–	265.588	$3p3d \ ^1D_2$	–	$3s3p^2(^3P)3d \ ^3P_1$	4.161E+05	1.063E+06	4.261E+05	1.056E+06	C1996
3	907.32	0.02	154.211	–	264.430	$3p3d \ ^1D_2$	–	$3s3p^2(^3P)3d \ ^3P_2$	6.558E+06	1.852E+07	7.711E+06	1.969E+07	C1996
2	948.98	0.01	16.299	–	121.675	$3p^2 \ ^1D_2$	–	$3s3p^3 \ ^3D_2$	6.886E+05	3.534E+05	7.340E+05	3.857E+05	C1995
2	949.38	0.01	16.299	–	121.629	$3p^2 \ ^1D_2$	–	$3s3p^3 \ ^3D_1$	6.864E+05	6.919E+05	7.913E+05	7.149E+05	C1995
[5]	1194.528	0.002	37.912	–	121.629	$3p^2 \ ^1S_0$	–	$3s3p^3 \ ^3D_1$	7.534E+04	2.682E+04	7.701E+04	2.996E+04	R1992
1d	1202.39	0.02	195.356	–	278.523	$3s3p^3 \ ^1P_1$	–	$3s3p^2(^1D)3d \ ^1D_2$	1.841E+07	1.447E+08	1.754E+07	1.557E+08	C1996
1	1341.68	0.02	191.537	–	266.075	$3s3p^3 \ ^3S_1$	–	$3s3p^2(^3P)3d \ ^3P_0$	6.724E+06	4.691E+07	8.810E+06	5.051E+07	C1996
5	1350.43	0.02	191.537	–	265.588	$3s3p^3 \ ^3S_1$	–	$3s3p^2(^3P)3d \ ^3P_1$	1.976E+07	1.361E+08	2.590E+07	1.466E+08	C1996
5	1371.92	0.02	191.537	–	264.430	$3s3p^3 \ ^3S_1$	–	$3s3p^2(^3P)3d \ ^3P_2$	3.365E+07	2.209E+08	4.385E+07	2.377E+08	C1996
2	1413.97	0.02	195.356	–	266.075	$3s3p^3 \ ^1P_1$	–	$3s3p^2(^3P)3d \ ^3P_0$	1.280E+05	4.596E+05	1.702E+05	4.529E+05	C1996
1	1447.66	0.02	195.356	–	264.430	$3s3p^3 \ ^1P_1$	–	$3s3p^2(^3P)3d \ ^3P_2$	1.308E+06	2.158E+06	1.735E+06	2.084E+06	C1996
New Lines													
2q	479.83	0.02	16.299	–	224.706	$3p^2 \ ^1D_2$	–	$3p3d \ ^3D_3$	2.874E+08	1.551E+08	3.028E+08	1.614E+08	New
1	607.01	0.02	265.588	–	430.331	$3s3p^2(^3P)3d \ ^3P_1$	–	$3p5s \ ^3P_1$	2.892E+06	2.636E+07	4.657E+05	2.604E+07	New
3bl	796.99	0.02	16.299	–	141.771	$3p^2 \ ^1D_2$	–	$3s3p^3 \ ^3P_1$	2.753E+06	1.647E+06	2.952E+06	1.760E+06	New
2q bl C III <sup>c</sup>	1175.25	0.02	0.763	–	85.851	$3p^2 \ ^3P_1$	–	$3s3p^3 \ ^5S_2$	1.333E+05	1.243E+05	1.438E+05	1.298E+05	E1963
4w bl C I <sup>c</sup>	1193.02	0.02	2.029	–	85.851	$3p^2 \ ^3P_2$	–	$3s3p^3 \ ^5S_2$	3.493E+05	3.302E+05	3.756E+05	3.449E+05	F1976
2	1423.91	0.02	195.356	–	265.588	$3s3p^3 \ ^1P_1$	–	$3s3p^2(^3P)3d \ ^3P_1$	8.525E+05	2.822E+06	1.098E+06	2.837E+06	New
2	2432.99	0.01	224.498	–	265.588	$3p3d \ ^3D_2$	–	$3s3p^2(^3P)3d \ ^3P_1$	8.367E+05	1.632E+06	1.001E+06	1.546E+06	New
3	3011.55	0.01	245.328	–	278.523	$3p3d \ ^1F_3$	–	$3s3p^2(^1D)3d \ ^1D_2$	2.948E+05	1.246E+04	2.584E+05	1.007E+04	New
1	3143.53	0.01	264.430	–	296.231	$3s3p^2(^3P)3d \ ^3P_2$	–	$3p4s \ ^3P_1$	1.385E+05	9.368E+04	1.455E+05	8.998E+04	New
2	3262.33	0.01	265.588	–	296.231	$3s3p^2(^3P)3d \ ^3P_1$	–	$3p4s \ ^3P_1$	7.412E+04	5.320E+04	7.766E+04	5.104E+04	New
6	4241.29	0.01	301.290	–	324.862	$3p4s \ ^1P_1$	–	$3s3p^2(^1D)3d \ ^1S_0$	7.554E+05	5.790E+04	7.985E+05	6.775E+04	New
3	4391.16	0.01	278.523	–	301.290	$3s3p^2(^1D)3d \ ^1D_2$	–	$3p4s \ ^1P_1$	1.813E+05	3.031E+05	1.778E+05	2.913E+05	New

**Notes.**

<sup>a</sup> Transition from an excited state,  $j$ , of energy,  $E_j$ , to a state,  $i$ , of lower energy,  $E_i$ , as defined in TASS, p. 395.

<sup>b</sup> The intensities of the lines are visual estimates of plate blackening, ranging from 1 to 5. The lines were not observed in our experiment when the intensity out of brackets is absent. Intensities in square brackets are from the National Institute of Standards and Technology (NIST) database (Kramida et al. 2018). Following NIST definitions: \* intensity is shared by several lines (typically, for multiply classified lines); bl blended with another line that may affect the wavelength and intensity; d is the diffuse line; q is the asymmetric line; t is the tentatively classified line; and w is the wide line.

<sup>c</sup> These possible Ar V transitions are blended by carbon lines. See Section 4.7.

**References.** C1995: Cavalcanti et al. (1995), C1996: Cavalcanti et al. (1996), E1963: Edlén (1963), F1978: Fawcett et al. (1978), F1976: Feldman et al. (1976), J1984: Jiang et al. (1984), L1984: Lévêque et al. (1984), P1941: Phillips & Parker (1941), and R1992: Raassen et al. (1992).

**Table 3**  
Energy Levels and Lifetimes of Ar V

Designation	LSJ	Exp. Values ( $10^3 \text{ cm}^{-1}$ )	Fitted ( $10^3 \text{ cm}^{-1}$ )	Composition <sup>a</sup>	Lifetime (ns)					
					HFR+CP Adjusted	HFR+CP	HFR Adjusted	HFR	Froese Fischer et al. (2006)	
$3p^2$	$^3P_0$	0.000	-0.022	93.6% $^3P$ + 2.4% $3s3p^2(^1D)3d^3P$						
	$^3P_1$	0.763	0.750	93.8% $^3P$ + 2.4% $3s3p^2(^1D)3d^3P$					1.573 s	
	$^3P_2$	2.029	2.034	93.4% $^3P$ + 2.4% $3s3p^2(^1D)3d^3P$					47.46 s	
	$^1D_2$	16.299	16.348	93.6% $^1D$ + 3.7% $3s3p^2(^3P)3d^1D$					1.595 s	
	$^1S_0$	37.912	37.893	93% $^1S$ + 4.3% $3p^4^1S$					106.7 ms	
$3s3p^2(^3P)3d$	$^3P_2$	264.430	264.550	66.4% $^3P$ + 21.5% $3p^4^3P$ + 9.1% $3s3p^2(^1D)3d^3P$	3.701	0.666	3.258	0.630	0.637	
	$^3P_1$	265.588	265.543	66.4% $^3P$ + 21.2% $3p^4^3P$ + 9% $3s3p^2(^1D)3d^3P$	3.703	0.665	3.260	0.629	0.634	
	$^3P_0$	266.075	266.002	66.1% $^3P$ + 21.1% $3p^4^3P$ + 8.9% $3s3p^2(^1D)3d^3P$	3.700	0.664	3.261	0.628	0.630	
$3s3p^2(^1D)3d$	$^1D_2$	278.523	278.521	47.8% $^1D$ + 38.3% $3p^4^1D$ + 5.9% $3s3p^2(^1S)3d^1D$	1.901	1.070	1.701	1.020	1.016	
	$^1S_0$	324.862	324.862	58.9% $^1S$ + 27.5% $3p^4^1S$ + 5.4% $3d^2^1S$	1.804	0.734	1.475	0.695	0.615	
$3s3p^2(^3P)3d$	$^1F_3$	411.173	411.171	44.1% $^1F$ + 34.7% $3p^4^1F$ + 15.1% $3s3p^2(^1D)3d^1F$	0.034	0.037	0.030	0.037		
$3p^24s$	$^5P_1$	<sup>b</sup> 394.551	394.629	98.2% $^5P$	0.168	0.166	0.169	0.172		
	$^5P_2$	<sup>b</sup> 395.303	395.312	98.2% $^5P$	0.166	0.165	0.168	0.170		
	$^5P_3$	<sup>b</sup> 396.391	396.305	98.2% $^5P$	0.164	0.163	0.166	0.169		
$3s3p^3$	$^5S_2$	<sup>b</sup> 85.851	85.787	98.6% $^5S$	10.351 $\mu\text{s}$	10.996 $\mu\text{s}$	9.617 $\mu\text{s}$	10.528 $\mu\text{s}$	8.283 $\mu\text{s}$	
	$^3D_1$	121.629	121.702	84.3% $^3D$ + 12.8% $3p3d^3D$	4.389	4.766	4.229	4.368	3.926	
	$^3D_2$	121.675	121.734	84.3% $^3D$ + 12.7% $3p3d^3D$	4.446	4.814	4.285	4.413	3.983	
	$^3D_3$	121.803	121.839	84.6% $^3D$ + 12.7% $3p3d^3D$	4.544	4.902	4.381	4.496	4.084	
	$^3P_2$	141.763	141.716	84.5% $^3P$ + 12.1% $3p3d^3P$	1.458	1.401	1.397	1.300	1.215	
	$^3P_1$	141.771	141.750	85% $^3P$ + 12% $3p3d^3P$	1.419	1.364	1.358	1.266	1.184	
	$^3P_0$	141.893	141.754	85.2% $^3P$ + 11.9% $3p3d^3P$	1.404	1.350	1.343	1.253	1.168	
	$^1D_2$	154.211	154.138	46.8% $^1D$ + 48.5% $3p3d^1D$ + 2.2% $3p^3(^2D)3d^1D$	1.208	1.364	1.197	1.227	1.175	
	$^3S_1$	191.537	191.513	88.5% $^3S$ + 5.6% $3p^3(^2D)3d^3S$ + 4% $3s3p^3^1P$	0.050	0.044	0.048	0.042	0.046	
	$3p3d$	$^1P_1$	195.356	195.528	76.3% $^1P$ + 14.8% $3p3d^1P$ + 4.5% $3s3p^3^3S$	0.094	0.085	0.090	0.082	0.091
		$^3P_2$	217.572	217.690	80.4% $^3P$ + 11.3% $3s3p^3^3P$	0.061	0.054	0.059	0.052	0.055
		$^3P_1$	218.287	218.260	82.7% $^3P$ + 11.5% $3s3p^3^3P$	0.061	0.053	0.059	0.051	0.054
		$^3P_0$	218.647	218.536	83.4% $^3P$ + 11.6% $3s3p^3^3P$	0.060	0.053	0.059	0.051	0.054
$^1D_2$		221.815	221.583	45.9% $^1D$ + 45.6% $3s3p^3^1D$ + 2.4% $3s3p3d^2(^1D)^1D$	0.047	0.041	0.045	0.040	0.042	
$^3D_1$		224.219	224.310	82% $^3D$ + 12.2% $3s3p^3^3D$	0.039	0.034	0.037	0.033	0.035	
$^3D_2$		224.498	224.566	81.8% $^3D$ + 12.1% $3s3p^3^3D$	0.039	0.034	0.038	0.033	0.035	
$^3D_3$		224.706	224.786	82.7% $^3D$ + 12.1% $3s3p^3^3D$	0.039	0.034	0.038	0.033	0.035	
$^1F_3$		245.328	245.094	94.7% $^1F$ + 2.1% $3s3p3d^2(^1G)^1F$	0.036	0.032	0.035	0.031	0.032	
$^1P_1$		252.141	252.345	80.2% $^1P$ + 13.5% $3s3p^3^1P$ + 3.3% $3p^3(^2P)3d^1P$	0.045	0.041	0.044	0.040	0.042	
$3p4s$	$^3P_0$	295.731	295.696	94.3% $^3P$	0.097	0.094	0.098	0.096	0.083	
	$^3P_1$	296.231	296.215	90.1% $^3P$ + 4.2% $3p4s^1P$	0.093	0.092	0.093	0.094	0.081	
	$^3P_2$	297.878	297.934	94.3% $^3P$	0.095	0.093	0.096	0.095	0.082	
$3p4d$	$^1P_1$	301.290	301.285	89.5% $^1P$ + 4.2% $3p4s^3P$	0.052	0.051	0.052	0.052	0.045	
	$^3D_2$	397.476	397.441	63.5% $^3D$ + 27.5% $3p4d^3F$ + 2.2% $3p4d^3P$	0.614	0.546	0.631	0.574		
	$^3D_1$	397.545	397.563	90.9% $^3D$ + 2.1% $3p^3(^2P)4d^3D$	0.567	0.498	0.601	0.538		
	$^3D_3$	397.800	397.814	62.1% $^3D$ + 29.6% $3p4d^3F$	0.621	0.552	0.638	0.579		
	$^3F_2$	398.987	398.937	58.5% $^3F$ + 25.6% $3p4d^3D$ + 9% $3p4d^1D$	0.659	0.552	0.655	0.571		
	$^3F_3$	399.487	399.451	62.5% $^3F$ + 30.7% $3p4d^3D$	0.671	0.560	0.666	0.579		

**Table 3**  
(Continued)

Designation	LSJ	Exp. Values ( $10^3 \text{ cm}^{-1}$ )	Fitted ( $10^3 \text{ cm}^{-1}$ )	Composition <sup>a</sup>	Lifetime (ns)				
					HFR+CP Adjusted	HFR+CP	HFR Adjusted	HFR	Froese Fischer et al. (2006)
3p5s	$^3P_2$	402.652	402.520	89.5% $^3P$ + 3%3p4d $^3D$ + 2.3%3p <sup>3</sup> ( $^2P$ )4d $^3P$	0.642	0.543	0.643	0.567	
	$^3P_1$	403.185	403.044	91% $^3P$ + 2.3%3p <sup>3</sup> ( $^2P$ )4d $^3P$	0.634	0.537	0.635	0.560	
	$^1F_3$	404.656	405.020	90.9% $^1F$ + 2.3%3p <sup>3</sup> ( $^2P$ )4d $^1F$	0.661	0.573	0.707	0.629	
	$^3P_1$	430.331	430.251	84.9% $^3P$ + 9.7%3p5s $^1P$	0.156	0.144	0.157	0.147	
	$^3P_2$	432.044	432.124	94.6% $^3P$ + 2.2%3p <sup>3</sup> ( $^2P$ )5s $^3P$	0.168	0.155	0.169	0.157	
	$^1P_1$	<sup>b</sup> 432.378	433.725	84.1% $^1P$ + 9.8%3p5s $^3P$	0.100	0.089	0.209	0.091	

**Notes.**

<sup>a</sup> We only show the three more significant and larger than 2% components.

<sup>b</sup> Levels not considered in the least-squares adjustment.

**Table 4**  
Least-squares Calculation for Even Parameters (Unities in  $\text{cm}^{-1}$ )

Config.	Parameter	HFR			HFR+CP		
		Theory	Adj.	Adj./Theory <sup>a</sup>	Theory	Adj.	Adj./Theory <sup>a</sup>
$3s^23p^2$	$E_{\text{av}}(3s^23p^2)$	30779	34606	3827	30891	34678	3787
	$F^2(3p, 3p)$	75872	64424	85%	76082	64597	85%
	$\zeta_{3p}$	1247	1437	115%	1253	1415	113%
$3s3p^23d$	$E_{\text{av}}(3s3p^23d)$	353699	339675	-14024	354056	340159	-13898
	$F^2(3p, 3p)$	76072	64144	84%	76220	65867	86%
	$\zeta_{3p}$	1267	1517	120%	1272	1467	115%
	$\zeta_{3d}$	50	50	100%	52	52	100%
	$F^2(3p, 3d)$	69859	75311	108%	70135	77254	110%
	$G^1(3s, 3p)$	102845	110008	107%	103077	106883	104%
	$G^2(3s, 3d)$	67603	72799	108%	67929	67787	100%
	$G^1(3p, 3d)$	87037	80754	93%	87311	86293	99%
$3p^4$	$E_{\text{av}}(3p^4)$	332030	374202	42164	332610	374674	42064
	$F^2(3p, 3p)$	75552	81594	108%	75674	81725	108%
	$\zeta_{3p}$	1248	1435	115%	1253	1416	113%
	$E_{\text{av}}(3p4p)$	364365	364365	0	365478	365478	0
$3p4p$	$\zeta_{3p}$	1361	1532	113%	1368	1539	113%
	$\zeta_{4p}$	322	322	100%	322	322	100%
	$F^2(3p, 4p)$	23017	23156	101%	23019	23019	100%
	$G^0(3p, 4p)$	6713	6754	101%	6715	6715	100%
	$G^2(3p, 4p)$	7662	7708	101%	7657	7657	100%
	$E_{\text{av}}(3s3p^24s)$	450489	451218	729	451741	452051	833
$3s3p^24s$	$F^2(3p, 3p)$	78164	72020	92%	78337	78337	100%
	$E_{\text{av}}(3p4f)$	447846	455216	7370	449195	449195	0
$3s^23p^2-3s3p^23d$	$R^1(3s, 3p; 3p, 3d)$	93267	106663	114%	93548	106984	114%
	$R^2(3s, 3p; 3d, 3p)$	70727	80886	114%	70967	81160	114%
$3s^23p^2-3p^4$	$R^1(3s, 3s; 3p, 3p)$	102189	116021	114%	102397	116257	114%
	$3s^23p^2-3s3p^24s$	$R^0(3s, 3s; 3s, 4s)$	5291	5274	99.7%	5306	5306
$R^1(3s, 3p; 3p, 4s)$		7792	7767	99.7%	7859	7859	100%
$R^0(3s, 3p; 4s, 3p)$		1425	1421	99.7%	1435	1435	100%
$R^1(3p, 3p; 3d, 3d)$		86759	85829	99%	87020	87020	100%
$3s^23p^2-3s^23d^2$	$R^3(3p, 3p; 3d, 3d)$	53566	54466	102%	53746	53746	100%
	$R^1(3s, 3d; 3p, 3p)$	93118	103284	111%	93358	103550	111%
$3s3p^23d-3p^4$	$R^1(3p, 3p; 3s, 3d)$	93254	92528	99%	93479	92751	99%

**Notes.** For the HFR calculation, the standard deviation obtained was  $66 \text{ cm}^{-1}$ . For HFR+CP, the standard deviation was  $79 \text{ cm}^{-1}$ . The table shows only parameters with values for adj./theory that are different from 100%, except in some cases.

<sup>a</sup> The values for  $E_{\text{av}}$  corresponds to the difference adj.-theory.

configuration as follows: the  $3p^4: {}^3P$  levels are now identified as  $3s3p^2({}^3P)3d: {}^3P$ , and the  $3p^4: {}^1D_2$  and  ${}^1S_0$  levels are now identified as  $3s3p^2({}^1D)3d: {}^1D_2$  and  ${}^1S_0$ , respectively. In that case, our calculations showed that there is only one case where the  $3p^4$  configuration corresponds to a dominant component, which is not observed yet, that is for the  $3p^4: {}^1S_0$  level, lying around  $430,000 \text{ cm}^{-1}$ . Table 7 shows the eigenvector components from the HFR+CP and least-squares-adjusted HFR+CP calculations for  $3p^4$  levels for comparison.

The discrepancy between our calculated values for  $3p^4$  lifetimes with that from Froese Fischer et al. (2006) was called to our attention. The most important reason is the different eigenvector composition produced by the adjusted energy parameters, as seen in Table 7. After the adjustment,  $3s3p^23d$  configuration components became dominant in all the analyzed

levels, enlarging lifetimes due to the values of the reduced matrix elements between  $3s3p^23d$  and  $3s3p^3$  being smaller than  $3p^4$  and  $3s3p^3$  and because the  $3p3d$  configuration differs from  $3p^4$  by three electrons (this is not the case for  $3s3p^23d$ ).

Not only lifetimes, but also the values of  $gA$  (and, therefore, of  $gf$ , see Equation (7)), are considerably different when calculated using adjusted parameters, being smaller for most transitions evolving  $3p^4$ , with consequences in the experimental analysis. Observations of the UV spectrum of the A35 nebula (Ziegler et al. 2012), a resolved binary system composed of a DAO-type white dwarf and its companion, found much lower  $f$  than those calculated for the transitions of  $3p^4: {}^3P_{j=0,1,2}-3s3p^3: {}^3S_1$ , with wavelengths of 1341.68, 1350.43, and 1371.92 Å. Those authors could not explain this disagreement between theoretical and empirical values, but

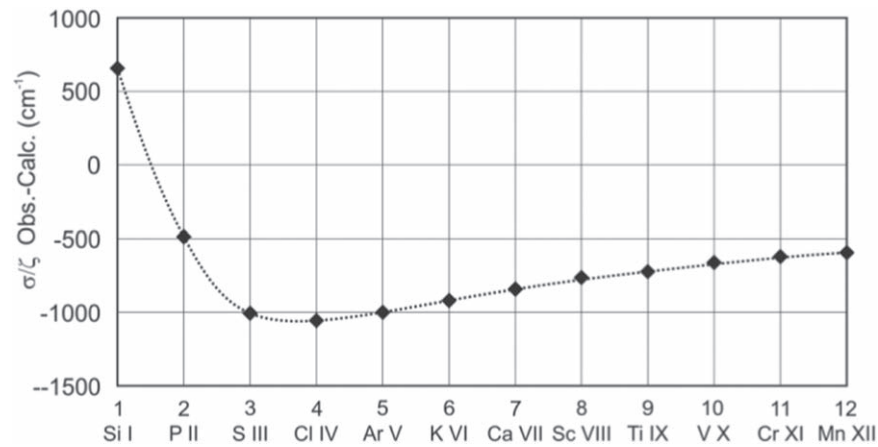


Figure 3. Isoelectric trend for the line at 479.83 Å.

**Table 5**  
Least-squares Calculation for Odd Parameters (Unities in  $\text{cm}^{-1}$ )

Config.	Parameter	HFR			HFR+CP		
		Theory	Adj.	Adj./Theory <sup>a</sup>	Theory	Adj.	Adj./Theory <sup>a</sup>
3s3p <sup>3</sup>	$E_{av}(3s3p^3)$	166992	163514	-3478	164828	164828	0
	$F^2(3p, 3p)$	75699	71114	94%	75862	68806	91%
	$\zeta_{3p}$	1247	1247	100%	1252	1193	95%
	$G^1(3s, 3p)$	102446	93670	91%	102703	96179	94%
3p3d	$E_{av}(3p3d)$	230249	223662	-6588	229561	222781	-6781
	$\zeta_{3p}$	1268	1268	100%	1275	1215	95%
	$\zeta_{3d}$	49	49	100%	51	51	100%
	$F^2(3p, 3d)$	69564	63049	91%	69857	62300	89%
	$G^1(3p, 3d)$	86598	77618	90%	86894	77058	89%
	$G^3(3p, 3d)$	53467	42774	80%	53671	42936	80%
3p4s	$E_{av}(3p4s)$	320725	318689	-2036	321802	318690	-3113
	$\zeta_{3p}$	1349	1551	115%	1356	1560	115%
	$G^1(3p, 4s)$	8050	6440	80%	8039	6862	85%
3p4d	$E_{av}(3p4d)$	423018	418366	-4652	424079	420278	-3801
	$\zeta_{3p}$	1354	1557	115%	1361	1565	115%
	$\zeta_{4d}$	16	16	100%	17	17	100%
	$F^2(3p, 4d)$	19507	18284	94%	19541	18394	94%
	$G^1(3p, 4d)$	8959	7167	80%	8880	7281	82%
	$G^3(3p, 4d)$	7264	5811	80%	7226	5926	82%
	$G^3(3p, 4d)$	7264	5811	80%	7226	5926	82%
3p <sup>3</sup> 3d	$E_{av}(3p^33d)$	506843	500858	-5985	507423	495356	-12067
	$F^2(3p, 3p)$	75885	68497	90%	75986	71214	94%
	$\zeta_{3p}$	1266	1456	115%	1271	1462	115%
	$\zeta_{3d}$	52	52	100%	54	54	100%
	$F^2(3p, 3d)$	70205	59674	85%	70472	62515	89%
	$G^1(3p, 3d)$	87521	74393	85%	87780	77870	89%
	$G^3(3p, 3d)$	54052	45944	85%	54236	48113	89%
	$G^3(3p, 3d)$	54052	45944	85%	54236	48113	89%
3p5s	$E_{av}(3p5s)$	456229	447730	-8500	447811	447710	-101
	$\zeta_{3p}$	1367	1572	115%	1374	1580	115%
	$G^1(3p, 5s)$	2653	2200	83%	2651	2199	83%
3s3p <sup>3</sup> -3p3d	$R^1(3p, 3p; 3s, 3d)$	92877	85462	92%	93141	85240	92%
3s3p <sup>3</sup> -3p <sup>3</sup> 3d	$R^1(3s, 3p; 3p, 3d)$	93526	84173	90%	93781	92933	99%
	$R^2(3s, 3p; 3d, 3p)$	70915	63823	90%	71140	70497	99%
3p3d-3p <sup>3</sup> 3d	$R^1(3s, 3s; 3p, 3p)$	102559	92303	90%	102732	82777	81%
3p4d-3p <sup>3</sup> 3d	$R^1(3s, 3s; 3p, 3p)$	105212	96795	92%	105400	110731	105%

**Notes.** For the HFR calculation, the standard deviation obtained was  $165 \text{ cm}^{-1}$ . For HFR+CP, the standard deviation was  $155 \text{ cm}^{-1}$ . The table shows only parameters with values for adj./theory that are different from 100%, except in some cases.

<sup>a</sup> The values for  $E_{av}$  corresponds to the difference in adj.-theory.

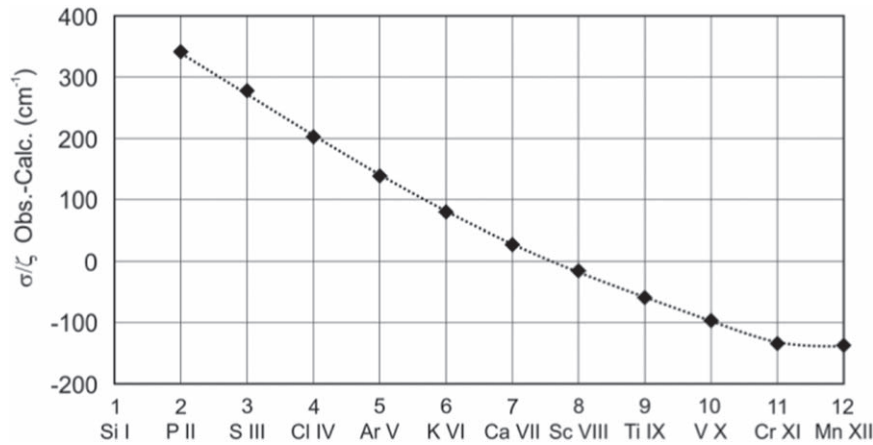


Figure 4. Isoelectric trend for the line at 796.99 Å.

Table 6  
Comparison with Experimental Lifetimes<sup>a</sup> for Ar V

Term	Livingston et al. (1981) Experimental	Froese Fischer et al. (2006)	HFR +CP (Adj.)	HFR+CP	
$3s3p^3$	$^3D$	$4.0 \pm 0.3$	4.02	4.44	4.84
	$^3P$	$1.2 \pm 0.1$	1.20	1.44	1.38
	$^1D$	$1.5 \pm 0.2$	1.18	1.21	1.36
	$^1P$	$0.12 \pm 0.02$	0.091	0.094	0.085
$3p3d$	$^3P$	$0.13 \pm 0.02$	0.054	0.060	0.053
	$^3D$	$0.03 \pm 0.01^b$	0.035	0.039	0.034
	$^1F$	$0.06 \pm 0.02^b$	0.032	0.036	0.032

Notes.

<sup>a</sup> Lifetime values are in ns.

<sup>b</sup> This value may represent only an upper limit (Livingston et al. 1981).

since their  $f$  values are very similar to ours when we calculate them without adjustment, we credit the low transition rates to the same reasons explained in the previous paragraph.

This abrupt change in the composition of the eigenvectors has its origin in the displacement of the average energies of the interacting configurations, a behavior that was also found in Kr V. The relative positions for  $3p^4$  and  $3s3p^23d$  average energies exchanges their values for both ions; while the theoretical value for  $3p^4$  is smaller than  $3s3p^23d$ , the adjusted values are just the opposite.

Therefore, in this study, we reclassified the  $3p^4$  levels as  $3s3p^23d$  for the reasons discussed here.

#### 4.7. The Metastable Level $3s3p^3:5S_2$ and the Classification of the Line 415.6 Å

The lowest energy level of the odd parity is the  $3s3p^3:5S_2$ . This level shows only intersystem transitions as decay channels. Its lifetime is of the order of  $10 \mu\text{s}$ , which is around ten thousand times greater than a typical lifetime for other electric dipole transitions. None of the Ar V lines observed has its initial state in this level, and its energy relative to the ground state is still dubious.

The fact that the level  $3s3p^3:5S_2$  is the lowest energy level of the odd parity means that many levels with multiplicity 5 or 7

(quintets or septets) of even parity will establish transitions with a relatively high probability of occurrence to this level. Therefore, in low-density plasmas where collisional depopulation is less important, radiative transitions from this level will constitute an essential channel of energy loss. Transitions of  $3s3p^3:5S_2$  to ground  $^3P_{j=1,2}$  levels of S III were observed in the symbiotic novae V1016 Cyg (Smith et al. 1984) and RR Telescopii (Doschek & Feibelman 1993; Young et al. 2011), in the Nova Aquilae 1982 (Snijders et al. 1987), and in the Io torus (Moos et al. 1983; Hall et al. 1994). Smith et al. (1984) mention a possible observation of the transition to the  $^3P_2$  level above the solar white-light limb of the quiet Sun (Doschek et al. 1976; Heise et al. 1995). We do not know any astrophysical observations of these transitions for other ions of the Si-like sequence, including Ar V.

There are two attempts for the location of the level  $3s3p^3:5S_2$  in Ar V structure: (1) in their study, Träbert et al. (1988) found the value  $85,900 \pm 80 \text{ cm}^{-1}$  as the most reasonable from a number of possible candidate lines for the pair of transitions,  $3s^23p^2:3P_{1,2}-3s3p^3:5S_2$ ; (2) an isoelectronic study carried out by Ellis & Martinson (1984) identified this level at approximately  $84,107.0 \text{ cm}^{-1}$ , which is a value that was later considered by Saloman (2010) as a reference in his analysis of a set of transitions between  $3s3p^3:5S_2-3s3p^2(^3P)4s:5P_{1,2,3}$  and  $3s3p^3:1D_2-3s3p^2(^3P)4s:5P_3$ . Saloman identified this last transition as a line observed by Lévêque et al. (1984) at  $415.6 \pm 0.1 \text{ Å}$ .

By analyzing the isoelectronic trend of this level, we found the Träbert et al. (1988) prediction much more acceptable than the value obtained by Ellis & Martinson (1984). This level is pure at about 99% along the isoelectronic sequence, and there is no reason to expect a deviation of about  $-2000 \text{ cm}^{-1}$  for Ar V from the dotted line interpolated from “obs.-calc.” data of the isoelectronic trend showed in Figure 7, which is a displacement that the prediction of Ellis & Martinson (1984) produces.

In our spectrograms, a C III line appears at the probable location of the expected  $3s^23p^2:3P_1-3s3p^3:5S_2$  transition at  $1175.25 \text{ Å}$ , while a C I line at  $1193.02 \text{ Å}$  should be over the  $3s^23p^2:3P_2-3s3p^3:5S_2$  transition, whose combination produces the value  $85,851 \text{ cm}^{-1}$  for the level  $3s3p^3:5S_2$ . Table 2

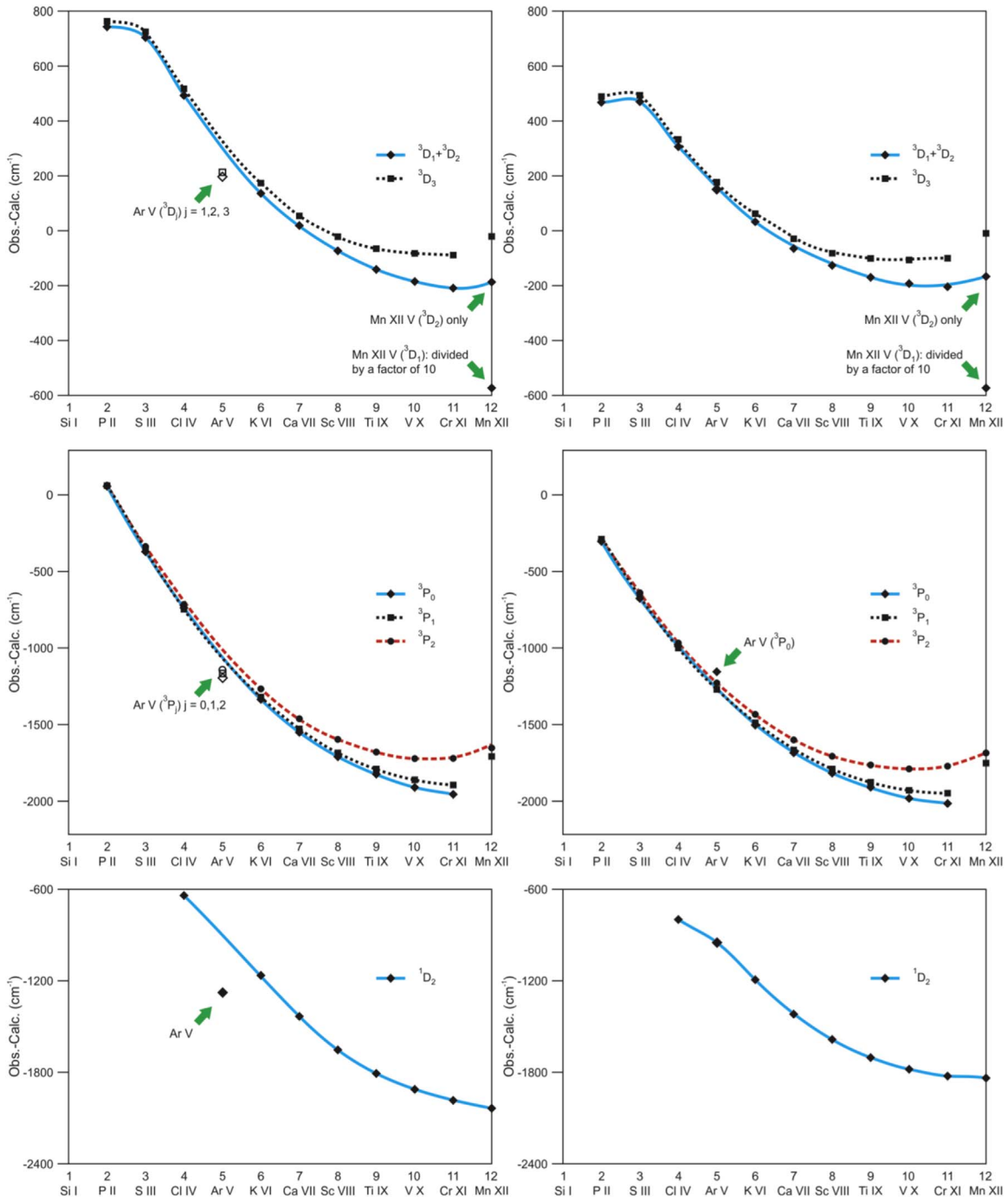


**Figure 5.** Isoelectric trend for the levels of the  $3s3p^3$  configuration. Left: without CP. Right: with CP.

identifies these transitions as carbon lines, but the composition and  $gA$  values are from the present Ar V calculation.

We leave the level  $^5S_2$  out of the least-square fitting. If included as a test, in the case HFR+CP, the result is much better for the  $85,851 \text{ cm}^{-1}$  value than for  $84,107 \text{ cm}^{-1}$ , which strengthens our choice (the difference between the adjusted and the experimental values is  $7 \text{ cm}^{-1}$  for this value and  $205 \text{ cm}^{-1}$  when we use  $84,107 \text{ cm}^{-1}$ ).

If the value  $85,851 \text{ cm}^{-1}$  is correct for the level  $^5S_2$ , the line  $415.6 \text{ \AA}$  (mentioned above) is misclassified, a hypothesis that is reinforced by the fact that the  $gA$  value for this line is too weak

(of the order of  $10^2\text{--}10^3 \text{ s}^{-1}$ ) when compared with the experimental observation. Another factor is that Lévêque et al. (1984) classified this line as Ar V but did not identify the three strong Ar VII lines in almost the same wavelength, which suggests that this line is, in fact, a superposition of Ar VII lines that could not be resolved by their instrument. The choice of  $85,851 \text{ cm}^{-1}$  as the correct value for the level  $3s3p^3: ^5S_2$  has as a consequence of the displacement of the value of the  $3s3p^2(^3P)4s: ^5P$  levels to  $394,551 \text{ cm}^{-1}$  ( $^5P_1$ ),  $395,303 \text{ cm}^{-1}$  ( $^5P_2$ ), and  $396,391 \text{ cm}^{-1}$  ( $^5P_3$ ). Although we did not include those levels in the final running of least-squares fitting, the

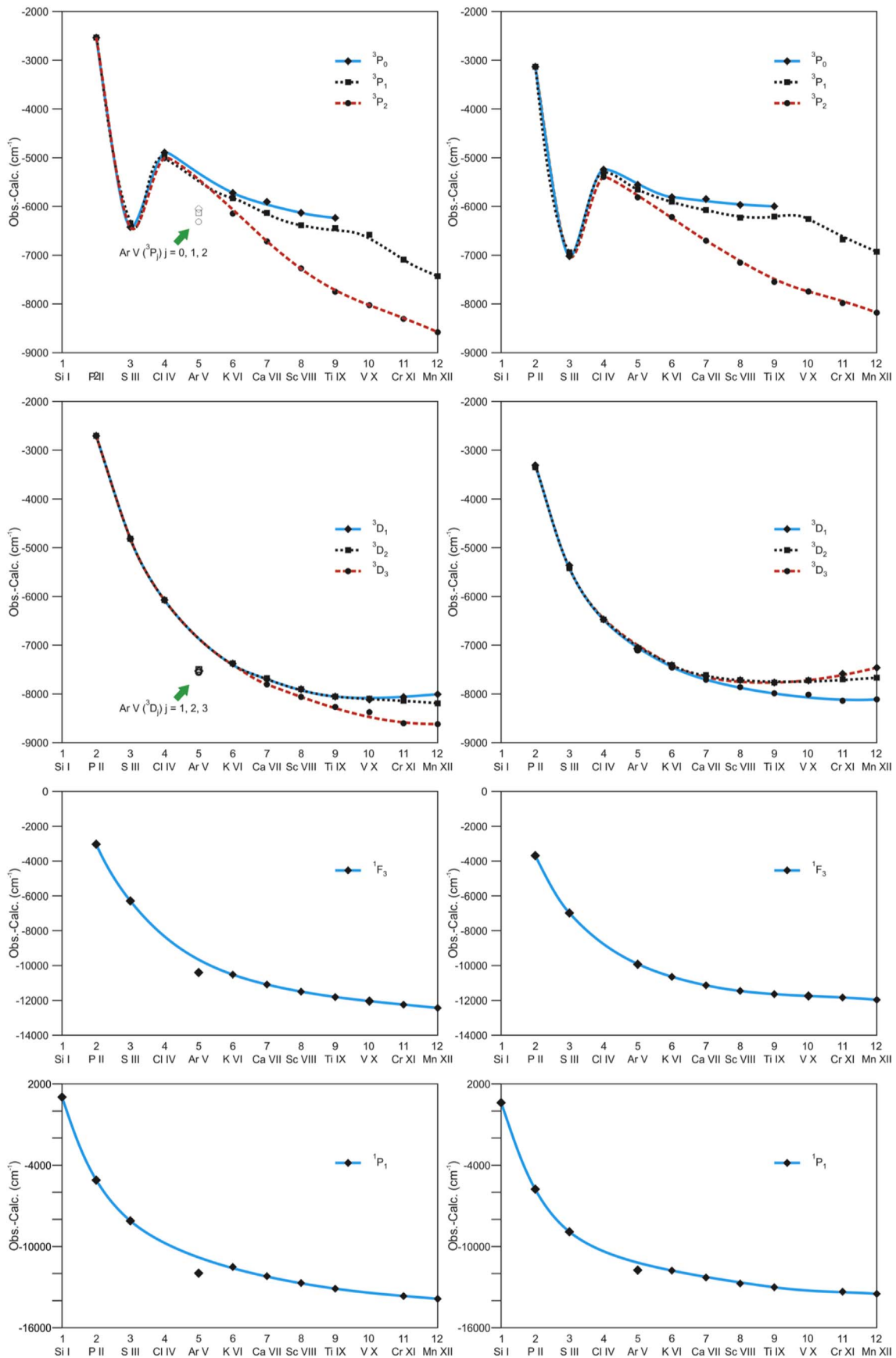
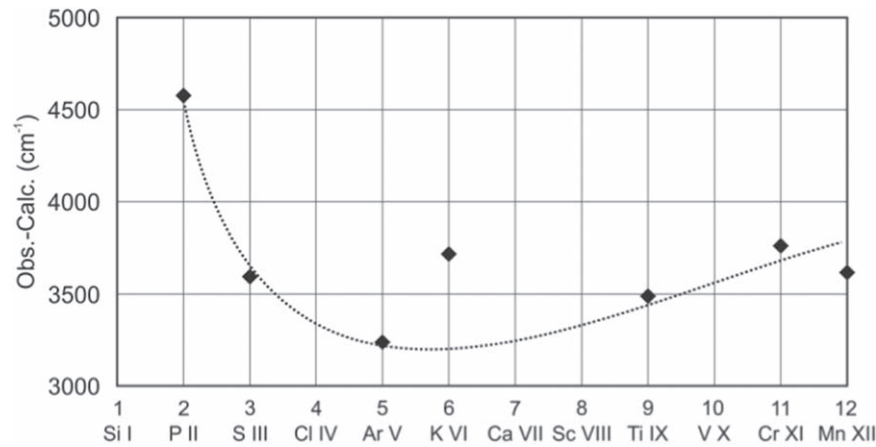


Figure 6. Isoelectric trend for the levels of the  $3p3d$  configuration. Left: without CP. Right: with CP.





**Figure 7.** Isoelectronic trend for the level  $3s3p^3:5S_2$ , with Ar V as predicted by Träbert et al. (1988) and adopted in this study at  $85,851 \text{ cm}^{-1}$ . If we adopt the value of Ellis & Martinson (1984), the point corresponding to Ar V will decrease about  $2000 \text{ cm}^{-1}$ , which is outside the range of this graph.

**Table 7**

Comparison between the Compositions and the Lifetimes Obtained from the HFR+CP Calculation and the HFR+CP Adjusted by Least-squares Procedure for  $3s3p^23d$  Levels

Exp. Values ( $10^3 \text{ cm}^{-1}$ )	Composition <sup>a</sup>	Lifetime (ns)		
		HFR+CP	HFR+CP Adjusted	Froese Fischer et al. (2006)
264.430	47.4% $3p^4 \ ^3P$ + 44.1% $3s3p^2(^3P)3d \ ^3P$ + 4.4% $3s3p^2(^1D)3d \ ^3P$	0.666	3.698	0.637
Adj.:	21.5% $3p^4 \ ^3P$ + 66.4% $3s3p^2(^3P)3d \ ^3P$ + 9.1% $3s3p^2(^1D)3d \ ^3P$			
265.588	47.5% $3p^4 \ ^3P$ + 44.7% $3s3p^2(^3P)3d \ ^3P$ + 4.4% $3s3p^2(^1D)3d \ ^3P$	0.665	3.700	0.634
Adj.:	21.2% $3p^4 \ ^3P$ + 66.4% $3s3p^2(^3P)3d \ ^3P$ + 9.0% $3s3p^2(^1D)3d \ ^3P$			
266.075	47.4% $3p^4 \ ^3P$ + 44.8% $3s3p^2(^3P)3d \ ^3P$ + 4.4% $3s3p^2(^1D)3d \ ^3P$	0.664	3.697	0.630
Adj.:	21.1% $3p^4 \ ^3P$ + 66.1% $3s3p^2(^3P)3d \ ^3P$ + 8.9% $3s3p^2(^1D)3d \ ^3P$			
278.523	57.4% $3p^4 \ ^1D$ + 32.5% $3s3p^2(^1D)3d \ ^1D$ + 3.7% $3s3p^2(^1S)3d \ ^1D$	1.070	1.901	1.016
Adj.:	38.3% $3p^4 \ ^1D$ + 47.8% $3s3p^2(^1D)3d \ ^1D$ + 5.9% $3s3p^2(^1S)3d \ ^1D$			
324.862	51% $3p^4 \ ^1S$ + 37.9% $3s3p^2(^1D)3d \ ^1S$ + 4% $3p^2 \ ^1S$	0.734	1.802	0.615
Adj.:	27.5% $3p^4 \ ^1S$ + 58.9% $3s3p^2(^1D)3d \ ^1S$ + 5.4% $3d^2 \ ^1S$			

**Note.**

<sup>a</sup> We show only the three more significant and larger than 2% components.

deviations remained smaller than  $80 \text{ cm}^{-1}$ , showing a good adjustment of the new experimental values to the calculated ones.

## 5. Conclusions

In the present work, the spectral analysis of Ar V was carried out, and new visible and ultraviolet lines were classified. In the analysis, least-squares calculations and studies of the isoelectronic trend were made. The isoelectronic analysis very well supported the new line classifications in the vacuum ultraviolet at 479.83 and 796.99 Å, while least-squares calculation and line intensity predictions provided information to a confident classification of the new ultraviolet and visible lines in which levels of the  $3s3p^23d$  (formerly classified as  $3p^4$ ) configuration participate. The inclusion of CP effects in the Hartree–Fock equations was crucial for the confirmation of most of the  $3s3p^3$  and  $3p3d$  levels.

However, some issues depend on additional efforts to be adequately overcome. This is the case of the  $3s3p^3:5S_2$  metastable level analysis, which seems to be close to the value predicted by Träbert et al. (1988), which, at the present stage of knowledge, depends on two lines that appear to be blended by emissions spectrum of carbon. This is a problem since carbon is

a frequent contributor to the astrophysical spectra where argon is present. The lines 1175.25 and 1193.02 Å, classified here as Ar V, should be regarded as an attempt until a detailed investigation in the region around 1200 Å of low-density argon plasma confirms that no other option of a pair of lines can replace them. These lines should have a wavenumber interval very close to  $1266 \text{ cm}^{-1}$ , have a rate of intensity of about 1:3, and have a wavelength not far from the 1175–1218 Å interval to be able to replace our choice.

Finally, much information could be confirmed if more data of the Si-like sequence were known. The lack of information for chlorine and ions above argon in the isoelectronic sequence is an issue that needs to be overcome for the consolidation of Ar V classifications done until today.

The authors would like to thank the anonymous reviewers for their valuable comments on this study. This research was supported by the Consejo Nacional de Investigaciones Científicas y Técnicas (CONICET), Argentina, and by the Coordenação de Aperfeiçoamento de Pessoal de Nível Superior (CAPES), Brazil. Support of the Comisión de Investigaciones Científicas de la Provincia de Buenos Aires (CIC), where M.R. is a researcher, is also gratefully acknowledged.

## ORCID iDs

C. J. B. Pagan  <https://orcid.org/0000-0002-3104-129X>

## References

- Baylis, W. E. 1977, *JPhB*, **10**, L583
- Biémont, É., Fischer, C. F., Godefroid, M. R., Palmeri, P., & Quinet, P. 2000a, *PhRvA*, **62**, 032512
- Biémont, É., Pinnington, E. H., Quinet, P., & Zeppen, C. J. 2000b, *PhyS*, **61**, 567
- Borges, F. O., Bredice, F., Cavalcanti, G. H., et al. 2005, *EPJD*, **36**, 23
- Bowen, I. S. 1935, *ApJ*, **81**, 1
- Bowen, I. S. 1960, *ApJ*, **132**, 1
- Boyce, J. C. 1935, *PhRv*, **48**, 396
- Cavalcanti, G. H., Luna, F. R. T., Trigueiros, A. G., et al. 1995, *Brazil J. Phys.*, **25**, 1, <http://sbfisica.org.br/bjp/download/v25/v25a01.pdf>
- Cavalcanti, G. H., Gallardo, M., Reyna Almandos, J. G., Gomide, J. V. B., & Trigueiros, A. G. 1996, *JPhB*, **29**, 6049
- Cowan, R. D. 1981, *The Theory of Atomic Structure and Spectra* (Berkeley, CA: Univ. California Press)
- Curtis, L. J. 2003, *Atomic Structure Lifetimes: A Conceptual Approach* (Berkeley, CA: Univ. California Press)
- Delgado-Inglada, G., Stasinska, C., & Morisset, G. 2014, *MNRAS*, **440**, 536
- Doschek, G. A., & Feibelman, W. A. 1993, *ApJS*, **87**, 331
- Doschek, G. A., Feldman, U., Van Hoosier, M. E., & Bartoe, J.-D. F. 1976, *ApJS*, **31**, 417
- Edlén, B. 1963, *RPPH*, **26**, 181
- Ellis, D. G., & Martinson, I. 1984, *PhyS*, **30**, 255
- Fawcett, B. C., Ridgeley, A., & Bromage, G. E. 1978, *PhyS*, **18**, 315
- Feldman, U., Brown, C. M., Doschek, G. A., Moore, C. E., & Rosenberg, F. D. 1976, *JOSA*, **66**, 853
- Feuchtgruber, H., Lutz, D., Beintema, D. A., et al. 1997, *ApJ*, **487**, 962
- Fraga, S., & Muszyńska, J. 1981, *Atoms in External Fields* (Amsterdam: Elsevier)
- Froese Fischer, C., Brage, T., & Johansson, P. 1997, *Computational Atomic Structure: An MCHF Approach* (London: CRC Press)
- Froese Fischer, C., Tachiev, G., & Irimia, A. 2006, *ADNDT*, **92**, 607
- Gallardo, M., Raineri, M., Reyna Almandos, J., Pagan, C. J. B., & Abrahão, R. A. 2015, *ApJS*, **216**, 1
- Hall, D. T., Bednar, C. J., Durrance, S. T., Feldman, P. D., & McGrath, M. A. 1994, *ApJL*, **420**, L45
- Heise, C., Smith, P. L., & Calamai, A. G. 1995, *ApJL*, **451**, L41
- Hibbert, A. 1975, *CoPhC*, **9**, 141
- Jiang, D.-Y., Shen, L.-K., Zhao, L.-Z., & Wang, W.-S. 1984, *ChJPh*, **33**, 508
- Johnson, W. R., Kolbt, D., & Huang, K.-N. 1983, *ADNDT*, **28**, 333
- Kelly, D. M., & Lacy, J. H. 1995, *ApJS*, **454**, L161
- Koch, V., & Andrae, D. 2011, *IJQC*, **111**, 891
- Kohstall, C., Fritzsche, S., Fricke, B., & Sepp, W.-D. 1998, *ADNDT*, **70**, 63
- Kramida, A., Ralchenko, Yu., Reader, J., & NIST ASD Team 2018, *NIST Atomic Spectra Database*, v. 5.6.1 (Gaithersburg, MD: NIST), <https://physics.nist.gov/asd>
- Levashov, V. E., & Struk, I. I. 1996, *QuEle*, **26**, 447
- Lévêque, G., Sébastien, G., & Robin, J. 1984, *J. Phys. France*, **45**, 665
- Livingston, A. E., Pinnington, E. H., Irwin, D. J. G., Kernahan, J. A., & Brooks, R. L. 1981, *JOSA*, **71**, 442
- McKenna, F. C., Keenan, F. P., Hambly, N. C., et al. 1997, *ApJS*, **109**, 225
- Migdalek, J., & Baylis, W. E. 1978, *JPhB*, **11**, L497
- Moos, H. W., Durrance, S. T., Skinner, T. E., et al. 1983, *ApJL*, **275**, L19
- Pagan, C. J. B., Cavalcanti, G. H., Jupén, C., & Trigueiros, A. G. 2011, *ApJS*, **196**, 19
- Penston, M. V., Benvenuti, P., Cassatella, A., et al. 1983, *MNRAS*, **202**, 833
- Phillips, L. W., & Parker, W. L. 1941, *PhRv*, **60**, 301
- Quinet, P., Palmeri, P., Biémont, É., et al. 1999, *MNRAS*, **307**, 934
- Quinet, P., Palmeri, P., Biémont, É., et al. 2002, *JALIC*, **344**, 255
- Raassen, A. J. J., Snoek, L. C., Volten, H., et al. 1992, *A&AS*, **95**, 223
- Raineri, M., Gallardo, M., Pagan, C. J. B., Trigueiros, A. G., & Reyna Almandos, J. 2012, *JQSRT*, **113**, 1612
- Raineri, M., Reyna Almandos, J., Amorim, E., Souza, J. O., & Fariás, E. E. 2017, *JPhCo*, **1**, 055022
- Rezende, D. C. J., Borges, F. O., Cavalcanti, G. H., et al. 2010, *JQSRT*, **111**, 2000
- Saloman, E. B. 2010, *JPCRD*, **39**, 033101
- Smith, P. L., Magnusson, C. E., & Zetterberg, P. O. 1984, *ApJL*, **277**, L79
- Snijders, M. A. J., Batt, T. J., Roche, P. F., et al. 1987, *MNRAS*, **228**, 329
- Stoy, R. H. 1934, *PASP*, **46**, 362
- Tayal, V., Gupta, G. P., & Tripathi, A. N. 2009, *InJPh*, **83**, 1271
- Träbert, E., Hutton, R., Engström, L., et al. 1988, *PhLA*, **129**, 381
- Werner, K., Rauch, T., & Kruk, J. W. 2007, *A&A*, **466**, 317
- Wright, W. H. 1920, *PASP*, **32**, 63
- Young, P. R., Feldman, U., & Lobel, A. 2011, *ApJS*, **196**, 23
- Ziegler, M., Rauch, T., Werner, K., Köppen, J., & Kruk, J. W. 2012, *A&A*, **548**, A109